2(mix)

NASA CR-122401

RADIO ASTRONOMY EXPLORER (RAE) I

OBSERVATIONS OF TERRESTRIAL RADIO NOISE

By

John R. Herman and Joseph A. Caruso

Analytical Systems Corporation

11 Ray Avenue

Burlington, Massachusetts

October 26, 1971

Contract No. NAS 5-11385

Prepared For

National Aeronautics and Space Administration

Goddard Space Flight Center

Greenbelt, Maryland 20771

1. Report No.	2. Government Accession No.	3. Recipient's Catalog No.

4. Title and Subtitle	5. Report Date
Radio Astronomy Explorer (RAE) I Observations of Terrestrial Radio Noise	October 26, 1971
	6. Performing Organization Code
7. Author(s)	8. Performing Organization Report No.
John R. Herman and Joseph A. Caruso	ASCR 72-54
9. Performing Organization Name and Address	10. Work Unit No.
Analytical Systems Corporation 11 Ray Avenue Burlington, Massachusetts 01803	
	11. Contract or Grant No.
	NAS5-11385
	13. Type of Report and Period Covered
12. Sponsoring Agency Name and Address	Type III (Final) 3/17/71 to 9/30/71
Dr. R. G. Stone, Code 693 NASA/GSFC Greenbelt, Maryland	14. Sponsoring Agency Code

15. Supplementary Notes

16. Abstract

Radio Astonomy Explorer (RAE) I data are analyzed to establish characteristics of HF terrestrial radio noise at an altitude of about 6000 km. Time and frequency variations in amplitude of the observed noise well above cosmic noise background are explained on the basis of temporal and spatial variations in ionospheric critical frequency coupled with those in noise source (thunderstorm activity) distributions. It is shown that terrestrial noise regularly breaks through the ionosphere and reaches RAE with magnitudes 15 or more dB higher than cosmic noise background. Maximum terrestrial noise is observed when RAE is over the dark side of the Earth in the neighborhood of equatorial continental land masses where thunderstorms occur most frequently. The observed noise level is 30-40 dB lower with RAE over oceans.

17. Key Words (Selected by Author(s))	18. Distribution Statement
Radio noise, Ionosphere, Thunderstorm, Radio Propagation, Satellite.	

19. Security Classif. (of this report)	20. Security Classif. (of this page)	21. No. of Pages	22. Price*
Unclassified	Unclassified	78	

Analytical Systems CORPORATION (617) 272-7910
11 RAY AVENUE
BURLINGTON, MASSACHUSETTS 01803

RADIO ASTRONOMY EXPLORER (RAE) I

OBSERVATIONS OF TERRESTRIAL RADIO NOISE

By

John R. Herman and Joseph A. Caruso

Analytical Systems Corporation

11 Ray Avenue

Burlington, Massachusetts

October 26, 1971

Contract No. NAS 5-11385

Prepared For

National Aeronautics and Space Administration

Goddard Space Flight Center

Greenbelt, Maryland 20771

ABSTRACT

Radio Astronomy Explorer (RAE) I data are analyzed to establish characteristics of HF terrestrial radio noise at an altitude of about 6000 km. Time and frequency variations in amplitude of the observed noise well above cosmic noise background are explained on the basis of temporal and spatial variations in ionospheric critical frequency coupled with those in noise source (thunderstorm activity) distributions. It is shown that terrestrial noise regularly breaks through the ionosphere and reaches RAE with magnitudes 15 or more dB higher than cosmic noise background. Maximum terrestrial noise is observed when RAE is over the dark side of the Earth in the neighborhood of equatorial continental land masses where thunderstorms occur most frequently. The observed noise level is 30-40 dB lower with RAE over oceans.

ACKNOWLEDGEMENTS

The RAE I data utilized in this investigation was supplied by National Aeronautics and Space Administration, Goddard Space Flight Center, through the courtesy of Dr. R. G. Stone. We acknowledge with appreciation, several helpful discussions with Dr. Stone regarding the analysis and the help extended by Mr. M. L. Kaiser of NASA/GSFC in reference to the data formats. Our appreciation also goes to Analytical Systems Corporation Staff Members, Dr. James Dillingham and Mr. Richard Vargas-Vila for a number of lively discussions.

TABLE OF CONTENTS

LIST OF FIGURES

1.0 INTRODUCTION

The radio noise environment within which a radio receiving system must operate is one of the main limiting performance factors for successful communications or data reception. An accurate knowledge of this environment is, therefore, required to assess the performance of receiving equipment both in satellites and on the ground.

Synoptic measurements of the atmospheric radio noise level at Earth's surface have been made for many years(Crichlow, et al, 1955; CCIR, 1957, 1964), but these are limited to land-based receivers widely scattered throughout the world while the ocean areas have been almost totally neglected. Thus, surface noise distributions as presently known contain large geographic areas of unverified noise level, and need to be improved. The contribution of terrestrial noise sources to the noise environment at satellite heights is even less well known, although some light has been shed on the problem through the works of Horner (1965), Huguenin and Papagiannis (1965) and Rawer (1967), among others.

The launching of Radio Astronomy Explorer (RAE) I on July 4, 1968 (Stone, 1969), has provided an opportunity to further investigate terrestrial radio noise characteristics both near Earth's surface and above the ionosphere. The objective of the research discussed in this report has been to analyze the RAE

noise data on frequencies near and above the ionospheric penetration (critical) frequency obtained on the dipole and downward Vee antennas (see Section 2.1) to isolate and identify the terrestrial noise contribution at the satellite and then to investigate its spatial, temporal and frequency characteristics.

Since the terrestrial noise characteristics as viewed by RAE I will be modified by the intervening ionosphere, it is necessary to consider the spatial and temporal variations of the ionosphere as well as the noise source distribution in analyzing the data. Appropriate ionospheric characteristics are discussed in Section 2 and terrestrial noise sources are treated in Section 3 as a prelude to the analysis results presented in Sections 4, 5 and 6.

2.0 RADIO PROPAGATION CONSIDERATIONS

Reception of terrestrially generated radio signals and noise by RAE I is a complex function of the observing frequency, satellite orientation and antenna characteristics, experiment geometry, ionospheric conditions and signal - or noise - source distributions over the Earth's surface. The characteristics of these various parameters are treated in this and the next Section in the context of how they may affect the RAE noise measurements.

2.1 RAE Characteristics

The satellite and its equipment are described in detail by Weber, Alexander and Stone (1971). Here we summarize only those features germane to the present effort.

The RAE I is in a retrograde, circular orbit at 5850 km with an inclination of 121° and a period of 3 hours 45 min., which allows it to cover geographic latitudes from 59°S to 59°N. Although the satellite itself remains in sunlight for six months of the year, it passes over the dark side of the Earth on each orbit.

It is equipped with a 37m dipole antenna coupled to a burst receiver (BR) which sweeps continuously through the frequency range 0.202 to 5.4 Megahertz (MHz) and two identical 230m Vee antennas connected to Ryle-Vonberg (RV) receivers.

Due to the gravity-stabilized orientation of RAE I one Vee antenna (upward Vee) continuously views the celestial sphere while the other (downward Vee) views the terrestrial sphere. The RV receivers operate at fixed frequencies from 0.45 to 9.18 MHz.

Both sweep frequency (BR) and fixed frequency (RV) data have been utilized in the present investigation, but principal attention has been confined to that for frequencies near and above the ionospheric critical frequency. In the BR data the frequency band considered is from about 2 to 5.4 MHz and for the RV the frequencies studied are 3.93, 4.70, 6.55 and 9.18 MHz.

2.2 Ionospheric Radio Propagation

The pertinent ionospheric characteristics are those leading to propagation effects (i.e. reflection, absorption or refraction) on radiowaves transmitted through the ionosphere from Earth's surface to RAE I.

On observing frequencies lower than the critical frequency (foF2) the signal is totally reflected below the F layer peak and no energy propagates to the satellite; the ground is thus shielded from the satellite and no terrestrial noise or signal would be received. The critical frequency varies with season, time-of-day, and geographic location, with a total range of about 1 MHz to 15 MHz. It would at times, shield all the

frequencies under consideration here and sometimes none of them. Grossly speaking, foF2 is high on the day side and low on the night side of the Earth in middle latitudes and higher in middle than polar or equatorial ($\pm$20°) latitudes. A typical diurnal variation in foF2 for a mid-latitude location is illustrated in Fig. 1. Note that the morning increase is much steeper than the afternoon and evening decline.

An idea of the geographic distribution of foF2 for two instants of time can be gained from the CRPL predicted median foF2 for 10 UT and 12 UT in December, 1968, reproduced in Fig. 2. (For later discussion an RAE I orbit is superimposed on the maps). Note in particular, the predicted 4-MHz low area in the northern hemisphere centered at a longitude of about 90°W at 10 UT, which can be seen to have moved westward two hours later at 12 UT. It is important to note that the illustrated maps are predicted monthly median values. On a day-to-day basis there is considerable fluctuation of foF2 about its median value, so prediction maps are best used as qualitative guides in determining the extent of ionospheric shielding. Specific examples of their use in analyzing RAE data are discussed in Section 4.

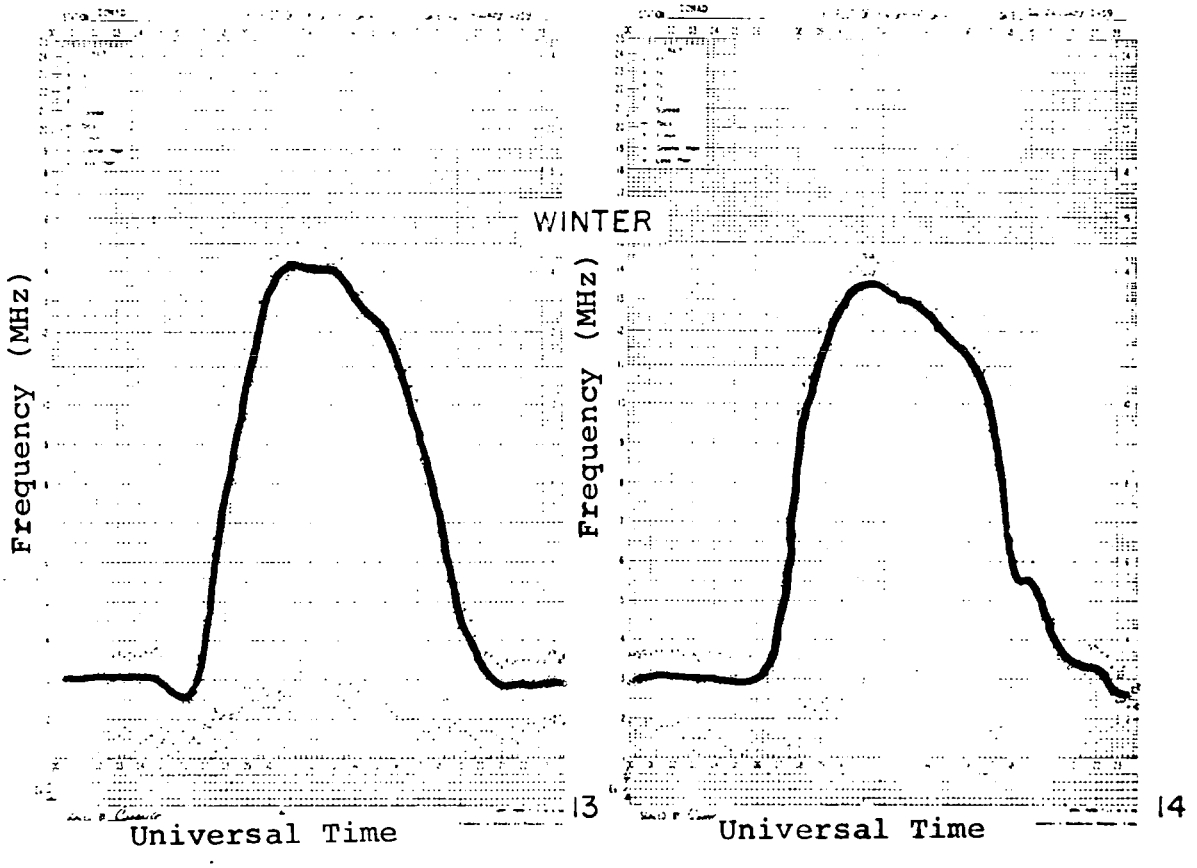

FIGURE 1 - TYPICAL DIURNAL VARIATION IN foF2 FOR TWO WINTER DAYS AT A MID-LATITUDE LOCATION (AFTER DAVIES, 1965).

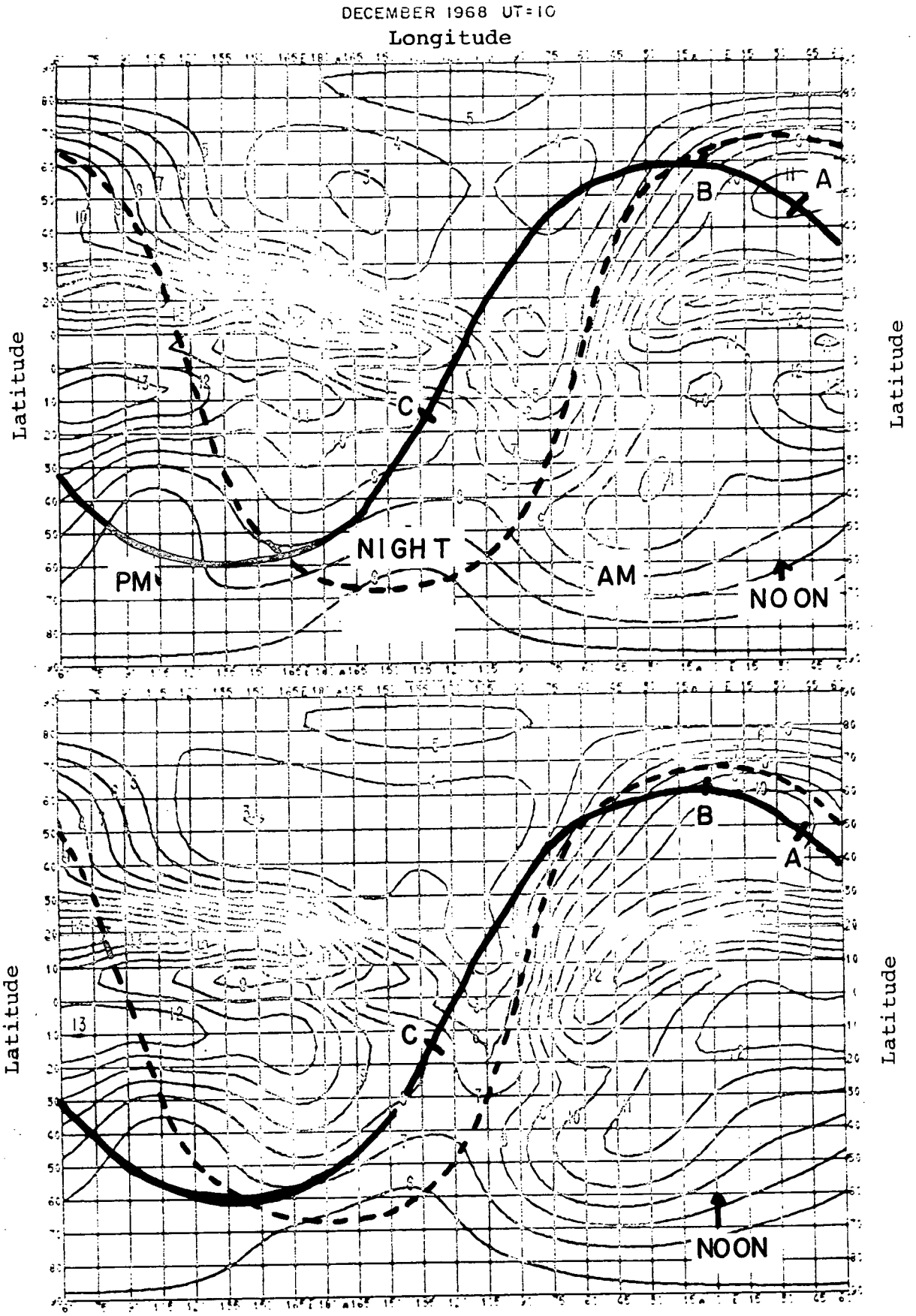

FIGURE 2 - PREDICTED MEDIAN foF2 (MHz) FOR DECEMBER, 1968, AT 10 UT (top) AND 12 UT (bottom) (AFTER ESSA, 1968). THE RAE ORBIT FOR DECEMBER 2, 1968, INCLUDING TIMES OF 1006 UT (POINT A) 1021 UT (B) AND APPROXIMATELY 1130 UT (C).

The spatial and temporal variations in shielding effects will follow approximately those in foF2 magnitudes, but the critical frequency alone is insufficient to describe the extent of shielding. It is only in the simplest case that noise or signals on frequencies barely above foF2 will penetrate the ionosphere at vertical incidence and be observed with RAE I directly overhead the source.

Generally speaking the penetration frequency depends upon the maximum plasma frequency of the F layer (foF2) and the angle of incidence of the radiowave entering the ionosphere.

An application of Snell's law yields the so-called Secant law for the total internal reflection.

$$f = foF2 \sec \phi_0$$

where foF2 = critical frequency of F2-layer

f = observing frequency

ϕ_0 = Angle of incidence measured from the normal to the F2 layer (see Fig. 3)

For a given observing and critical frequency, the ray will penetrate the ionosphere for any angle of incidence less than ϕ_0. Taking into consideration the fact that ϕ_0 is directly proportional to the observing frequency, one would expect the higher frequencies to be observed first as the satellite approaches the source, followed by the lower frequencies as

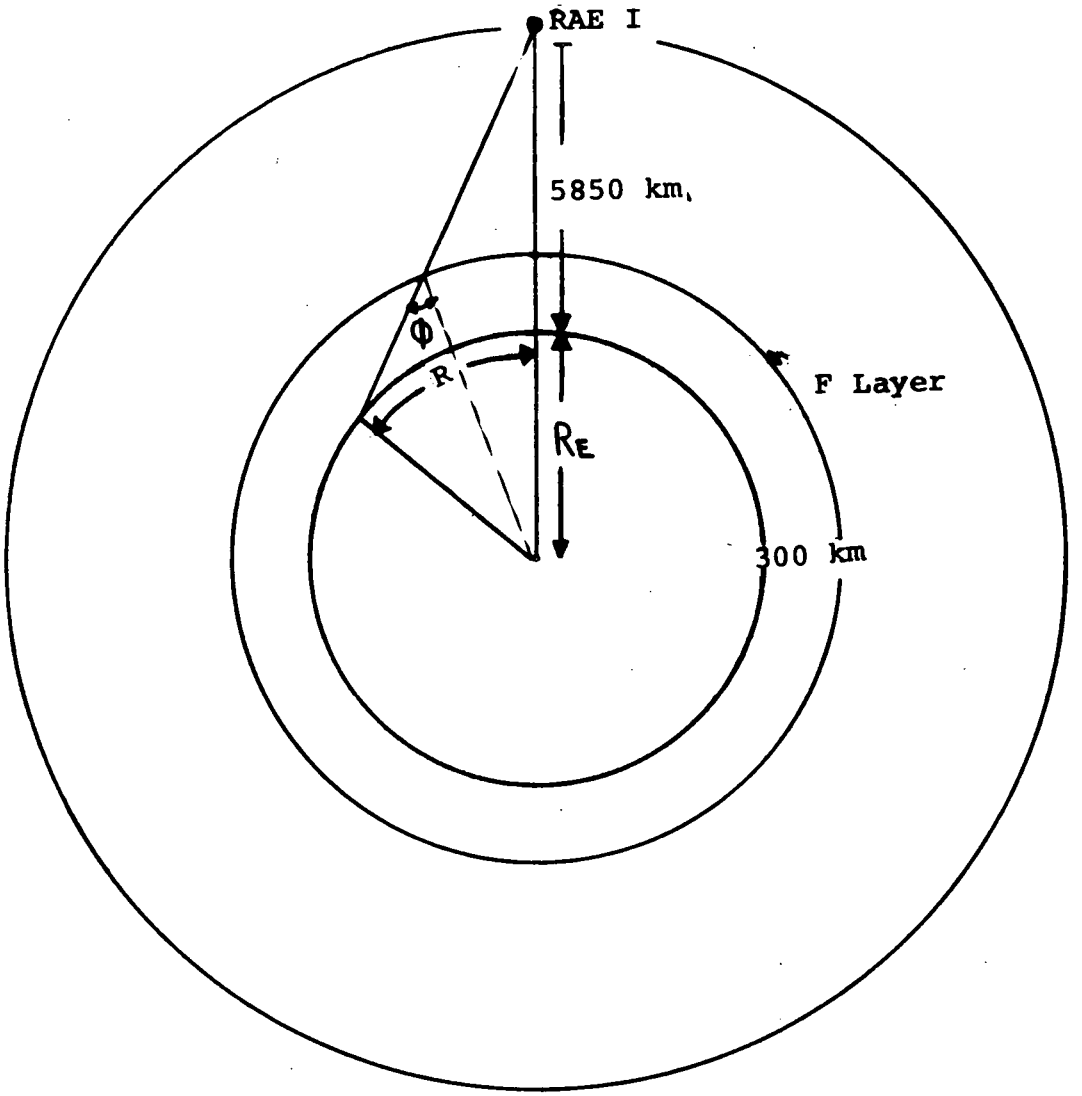

FIGURE 3 - GEOMETRY OF THE SATELLITE-GROUND SOURCE CONFIGURATION

the satellite moves closer to the source. As the satellite passes over the source and begins to move away, the lower frequencies will fade out first followed by the higher frequencies as the satellite-to-source distance increases. Consequently, the ionosphere acts as an "iris" whose size is directly proportional to the observing frequency and inversely proportional to the critical frequency.

In order to determine the relative size of the "iris" one can calculate the ground range R (Distance from subsatellite pt. to observable source) versus the ratio of ionospheric critical frequency (foF2) to observing frequency. The results of this calculation are displayed in Figure 4. Taking the limiting case, i.e. observing frequency = 9.2 MHz, foF2 = 3MHz, the ground range given in Figure 4 is 6450 km. As foF2/f increases, R decreases along with the "iris" size which is directly proportional to ground range. For example, with f = 3.2 MHz the ground range is 1000 km. It is clear that high frequencies see a much bigger "hole" in the ionosphere than the lower frequencies.

Refraction of radiowaves near the sides of the iris will enlarge its diameter to a certain extent depending upon frequency and the electron density distribution expressed in terms of radio refractive index. Qualitatively, magnetoionic theory predicts that for a specified ionosphere, the amount of

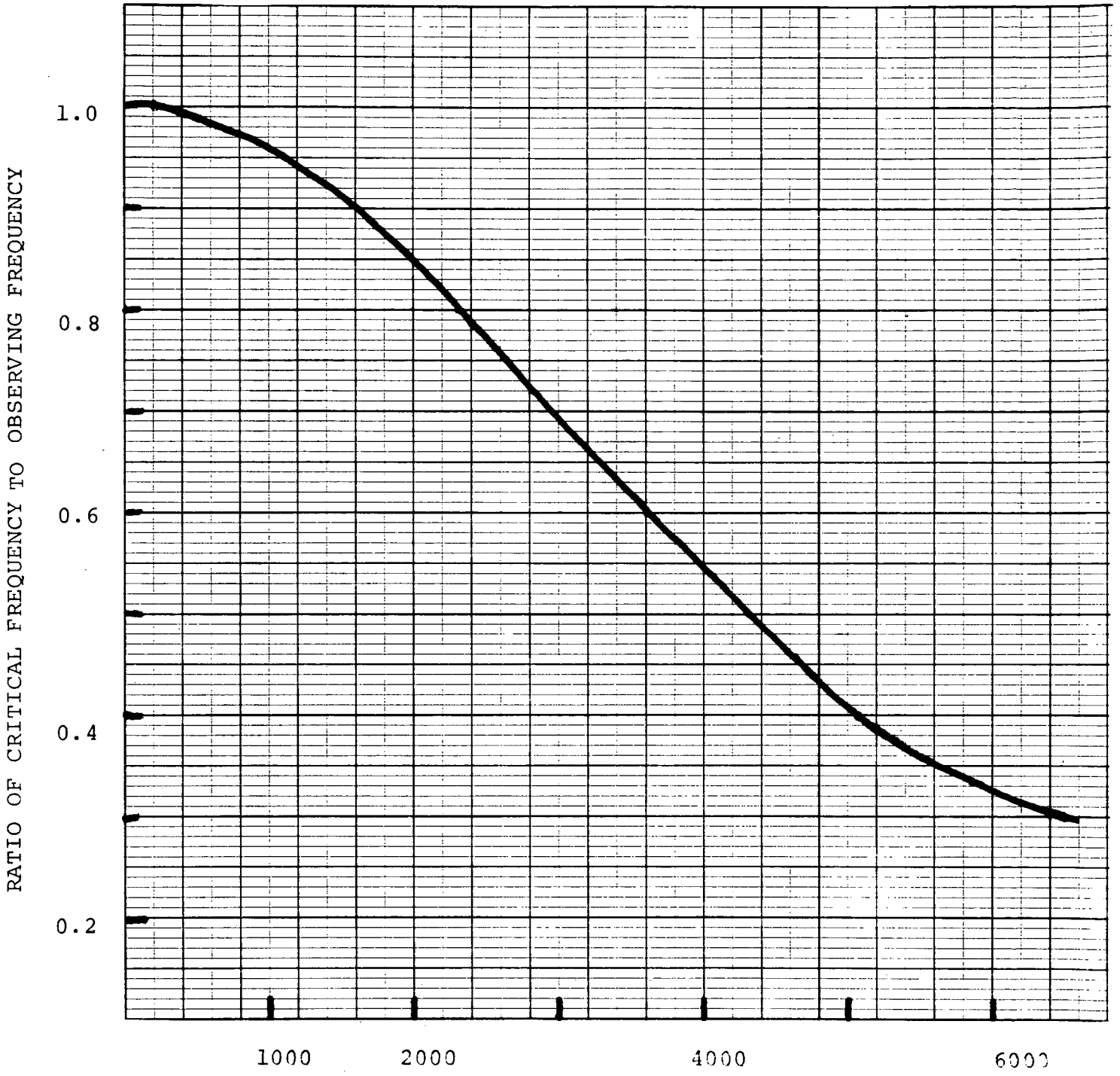

FIGURE 4 - RELATIONSHIP BETWEEN GROUND RANGE (R) SUB-SATELLITE POINT TO AN OBSERVABLE POINT SOURCE AND THE RATIO OF IONOSPHERIC CRITICAL FREQUENCY (foF2) TO OBSERVING FREQUENCY (R CORRESPONDS TO THE EFFECTIVE RADIUS OF THE IONOSPHERIC IRIS NEGLECTING REFRACTION).

refraction will increase with decreasing frequency at a given incidence angle, and that it will increase with increasing incidence angle on a fixed frequency. Quantitative refractive effects on signals propagating to RAE I have not been taken into account in the present investigation.

An additional large scale propagation effect of the ionosphere is the attenuation loss incurred in traversing the medium. The attenuation loss at vertical incidence due to D-region absorption is related to the frequency by (Herman, 1968)

$$L_V \text{ (dB)} = \frac{493}{(f+f_L)^2}$$

where f = observing frequency in Megahertz

f_L = longitudinal gyrofrequency in Megahertz ($\tilde{}$1MHz)

Assuming a plane ionosphere and neglecting the Earth's magnetic field, the attenuation loss at an angle of incidence ϕ is given approximately by (Davies, 1965)

$$L = L_V \sec \phi$$

Considering only the attenuating effect of the ionosphere, the loss increases with decreasing frequency and increasing angle of incidence. Therefore, at a given angle of incidence, one would expect the received power to increase with increasing frequency. Since a large part of the ionospheric attenuation stems from absorption in the D region, which is proportional

to the solar zenith angle, this loss is larger on the day side than the night side, and in equatorial than in temperate or polar latitudes.

Additional losses result from inverse square losses as a function of satellite position. Again, with the limiting case (see Fig. 4), the ratio of the distances squared yields

$$\frac{L_2}{L_1} = \frac{R_2^2}{R_1^2} = 2.92$$

This represents a difference in loss of approximately 5 dB.

Another factor which must be considered, is the area intercepted by the satellite antenna beamwidth projected down to the Earth's surface. The surface intercepted by the downward looking V-antenna operating at 9.2 MHz is elliptically shaped with semi-major and minor axes of 1400 km and 670 km respectively. The resulting area is approximately 3.00×10^6 km^2. This represents a region on the Earth's surface of approximately 10° of latitude by 28° of longitude or an area comparable to 1/3 the Australian Continent. The antenna beamwidth increases with decreasing frequency, with a corresponding increase in area.

The foregoing ionospheric propagation and experiment geometry considerations, combined with the noise source considerations discussed in Section 3, provide the framework within which the present data analysis has been conducted to derive the contribution of terrestrial noise sources to RAE measurements.

3.0 TERRESTRIAL RADIO NOISE

The principal source of terrestrially generated radio noise on frequencies of interest here are thunderstorm regions and metropolitan areas. Lightning and similar atmospheric electrical phenomena associated with thunderstorms generate electromagnetic radiation on frequencies from less than 10 kHz to more than 10MHz. Man-made radio noise is generated incidentally by electrical rotating and commutating devices, power lines, ignition systems and the like, and its magnitude can be greater than atmospheric radio noise in heavily populated urban and industrial areas. A third type of noise is unwanted signals from radio transmitters operating on discrete frequencies, but this type is generally referred to as "interference" rather than noise. This distinction is maintained in the present report.

Atmospheric and man made radio noise, like cosmic noise, are incoherent and therefore, add algebraically. Thus, when either is a factor of, say, 10 higher than cosmic noise, the effective noise level measured by RAE will be representative of the atmospheric or man made noise contribution with only small error, since the background cosmic noise under such conditions would be only a tenth of the total.

3.1 Man Made Radio Noise

The principal sources of man made radio noise are major metropolitan areas and are therefore concentrated on the continental land masses. Industrialized nations such as those in Europe and North America will contribute a greater amount to the overall man made noise environment than will those in Africa. Surface measurements in and near large cities such as New York, Seattle and Tokyo indicate that the man made level is much greater than that expected from atmospheric radio noise (in the absence of purely local thunderstorms) (c.f., Herman, 1969). However, the noise intensity falls off rapidly with distance away from the urban center in the lower HF frequency band appropriate to RAE 1 (Herman, 1969), and in "quiet" noise areas 15 to 20 km away,the atmospheric noise component apparently dominates. From the vantage point of RAE viewing, it is anticipated that urban noise will be important only over those regions of the world (such as the east coast of the United States, western industrialized Europe) where many urban population centers are concentrated so that several are within the antenna beamwidth simultaneously.

At present the data are too sparse to make a quantitative estimate of man made noise contributions to the noise level at RAE heights.

3.2 Radio Frequency Interference

Signals transmitted on frequencies greater than the ionospheric critical frequency can be received by RAE 1 in two ways. The first is directly from the transmitter through the ionospheric iris to the satellite. Looking at it from a ground-based propagation viewpoint, the maximum radius of the iris for a given frequency is approximately one-half the so-called "skip distance." The skip distance is the closest ground range where a ground-based receiver can receive the transmitted signal after one ionospheric reflection. At shorter ranges than that, the signal penetrates the ionosphere and is lost to the ground-based receiver, but it can reach RAE. At greater ranges the signal is reflected back to Earth.

The second way to receive ground-based transmissions at RAE is after the signal has propagated to large distances via ionospheric reflections to a point where its frequency exceeds foF2 and penetrates through the ionosphere.

Within the 2 to 10 MHz band of frequencies of interest, transmitted signals may originate in commercial broadcasts, private and military communications links, ham operators, navigation (Loran A) systems and the like. These are scattered throughout the world, principally on land in temperate and equatorial latitudes but also in some polar regions and on ships at sea. To estimate quantitatively

the geographic distribution of the rf energy in the form of interference at a given time, the locations of all operating transmitters, their radiated power and antenna patterns, along with propagation factors must be considered. Further, an estimate of the upward flux of ground-reflected or scattered energy is required in order to determine the quantitative contribution of interfering signals to the effective antenna temperature measured by RAE 1. Such a project is beyond the scope of the present effort, and may be impractical in any case. (A gross estimate of the relative importance of man made transmissions compared to atmospheric noise might be arrived at by summing up the radiated power of all known transmitters in the world, but this has not been done yet).

Few measurements have been made by rocket or satellite, but the results of Huguenin and Papagiannis (1965), indicate that at times, above the F region peak, interfering signals can be more than 50 dB stronger than cosmic noise.

In the analysis being reported on here, no attempt has been made to separate interference from other types of terrestrial noise viewed by RAE 1, except in isolated instances. It has been assumed, rather, that for the large scale spatial analysis being applied, the dominating influence is atmospheric radio noise.

3.3 Atmospheric Radio Noise

The spatial distribution of atmospheric radio noise sources can be approximated by the distribution of world wide thunderstorm activity. The number of thunderstorm days observed world wide in September, October, November and in December, January, February are given in Figs. 5 and 6 to illustrate atmospheric noise source distributions. From these it is obvious that thunderstorms occur much more often over the major continental land masses (Africa, the Americas, Asia) than over oceans.

The comparative areas and diurnal variations of the major noise sources (i.e. thunderstorm centers) are shown in Fig. 7. Here it is seen that the largest area is over Africa and Europe, next in size is the Americas and least is in Asia/Australia. In each case, the maximum area occurs generally in late afternoon local time. On a world-wide basis, maximum thunderstorm activity measured in area occurs between about 12 UT and 20 UT with the principal contribution coming from Africa/Europe and the Americas.

The median number of thunderstorms in progress at any 2-hour interval in the major source centers is shown in Fig. 8 for September, October and November. The maximums in these curves coincide with those in Fig.7. For fall equinox, more storms are in progress in Africa/Europe, than America or Asia. Curves

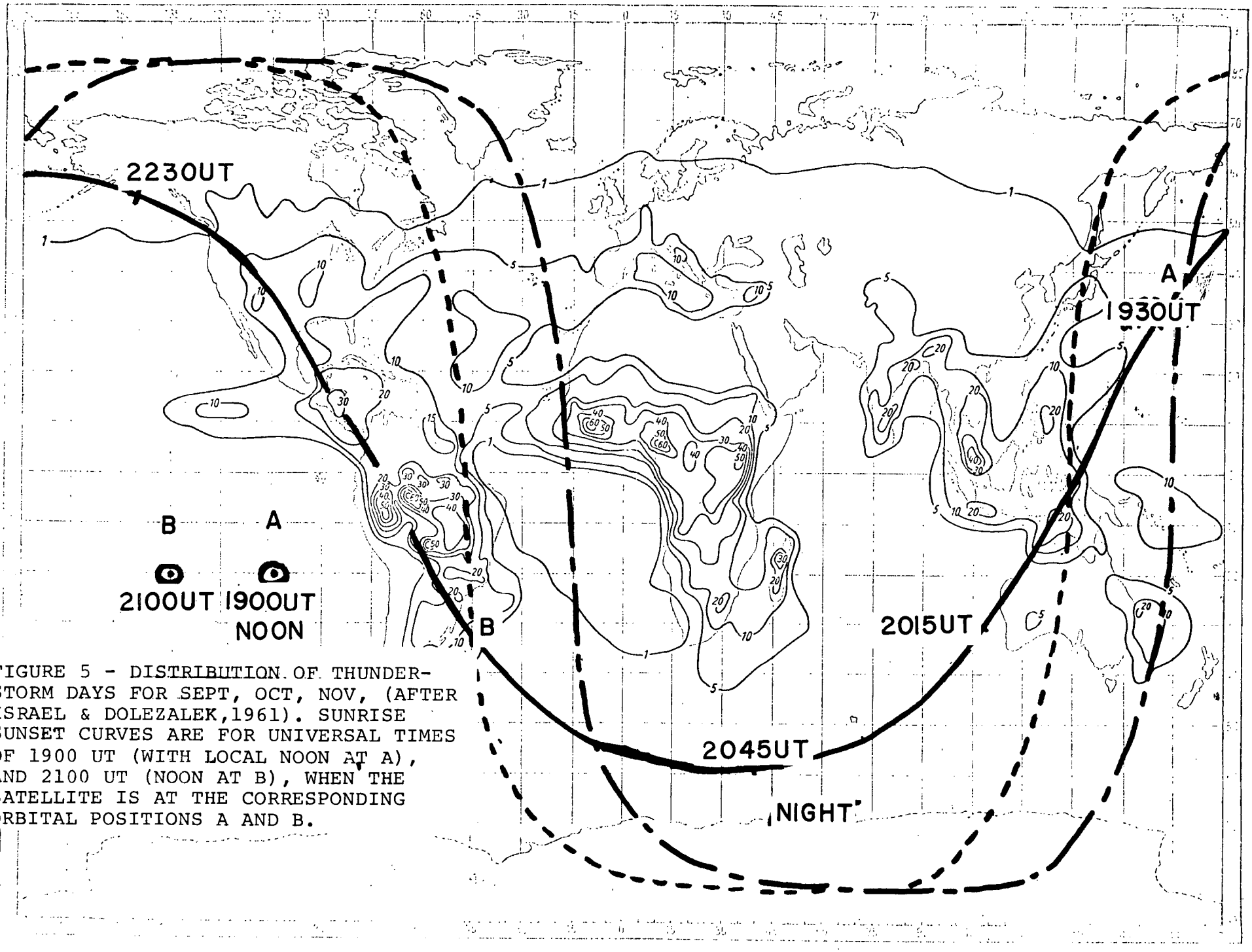

FIGURE 5 - DISTRIBUTION OF THUNDER-STORM DAYS FOR SEPT, OCT, NOV, (AFTER ISRAEL & DOLEZALEK,1961). SUNRISE SUNSET CURVES ARE FOR UNIVERSAL TIMES OF 1900 UT (WITH LOCAL NOON AT A), AND 2100 UT (NOON AT B), WHEN THE SATELLITE IS AT THE CORRESPONDING ORBITAL POSITIONS A AND B.

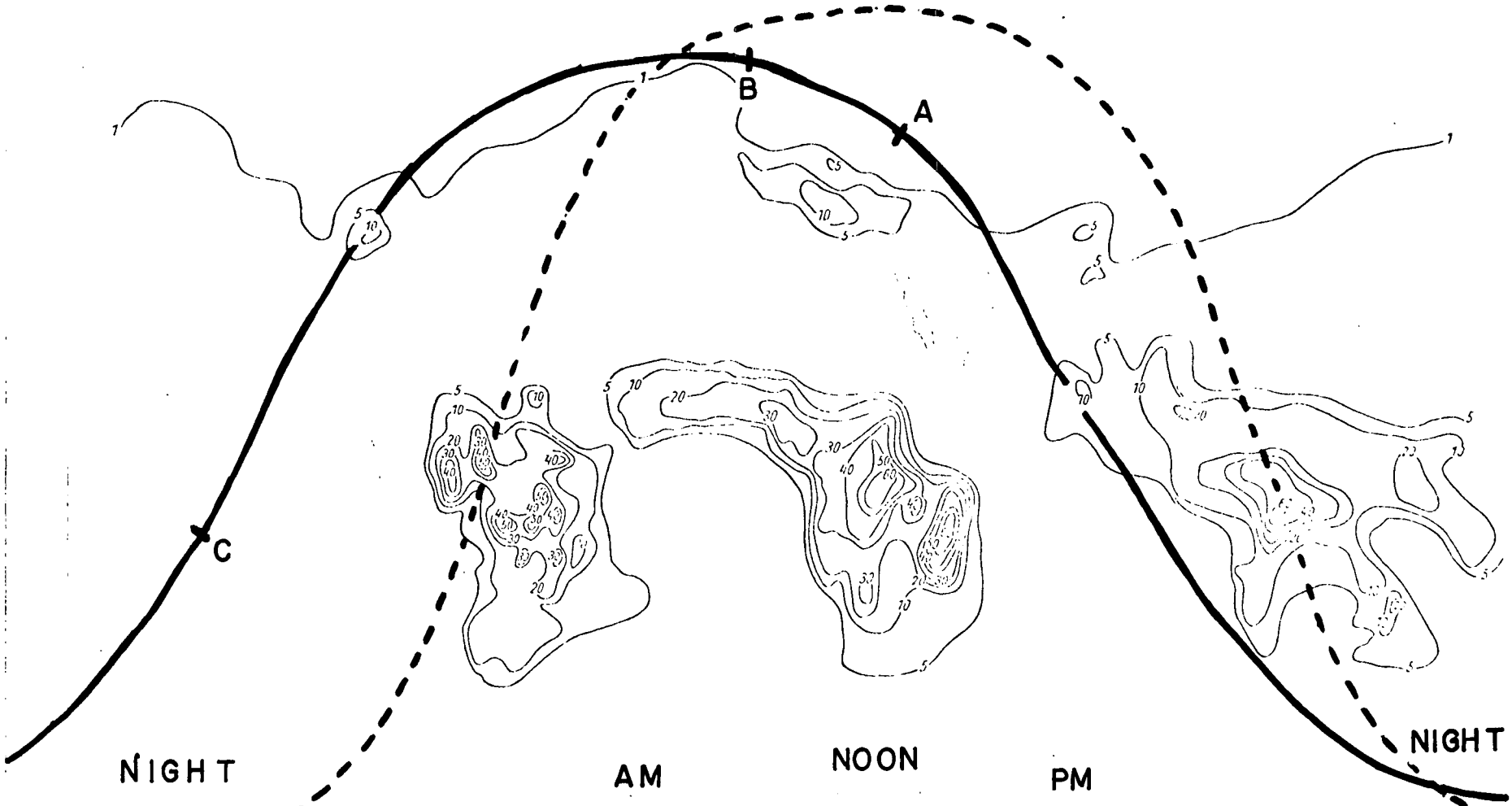

FIGURE 6 - DISTRIBUTION OF NUMBER OF THUNDERSTORM DAYS IN DEC, JAN, FEB, (AFTER ISRAEL & DOLEZALEK, 1961). THE TWILIGHT LINE FOR LOCAL NOON AT 30°E IS APPROPRIATE FOR THE ILLUSTRATED ORBIT APPROX.AT POINT A.

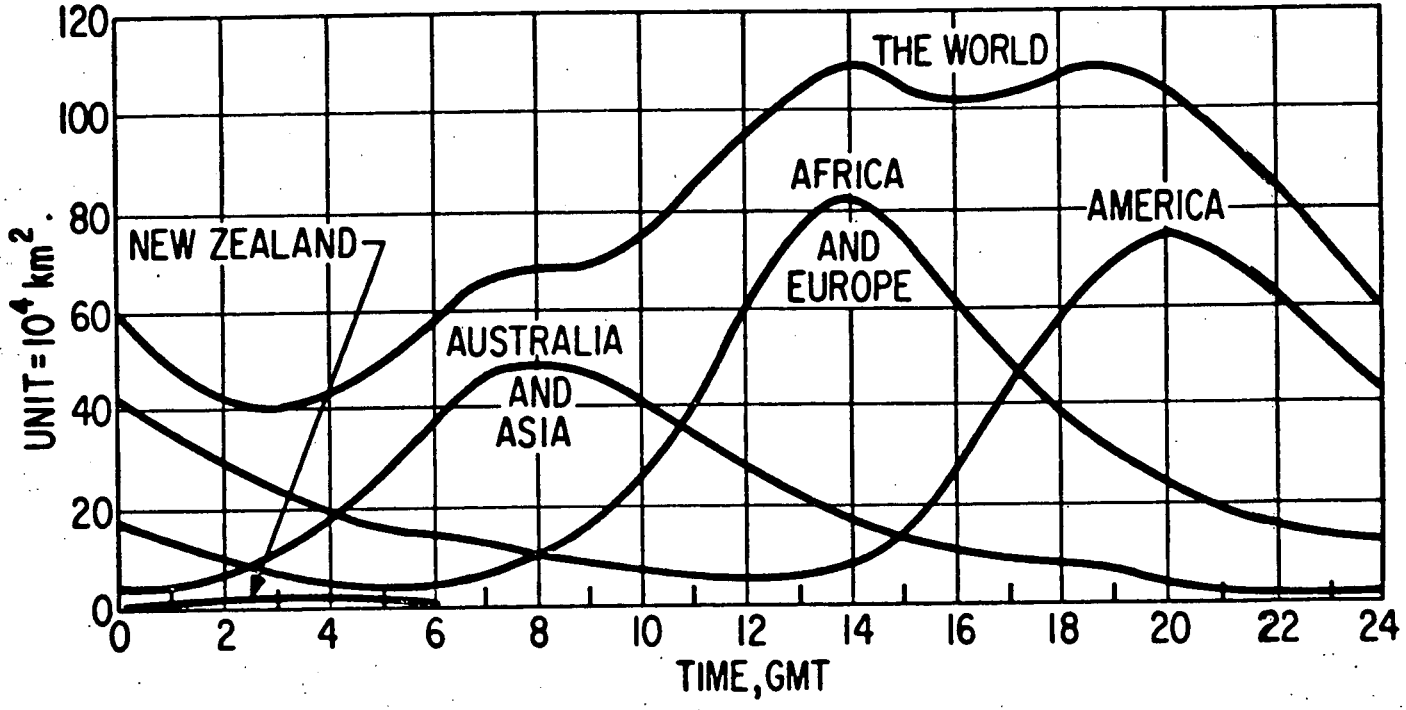

FIGURE 7 - DIURNAL DISTRIBUTION OF WORLD THUNDERSTORM ACTIVITY (AFTER WHIPPLE, 1929) IN TERMS OF SOURCE AREA

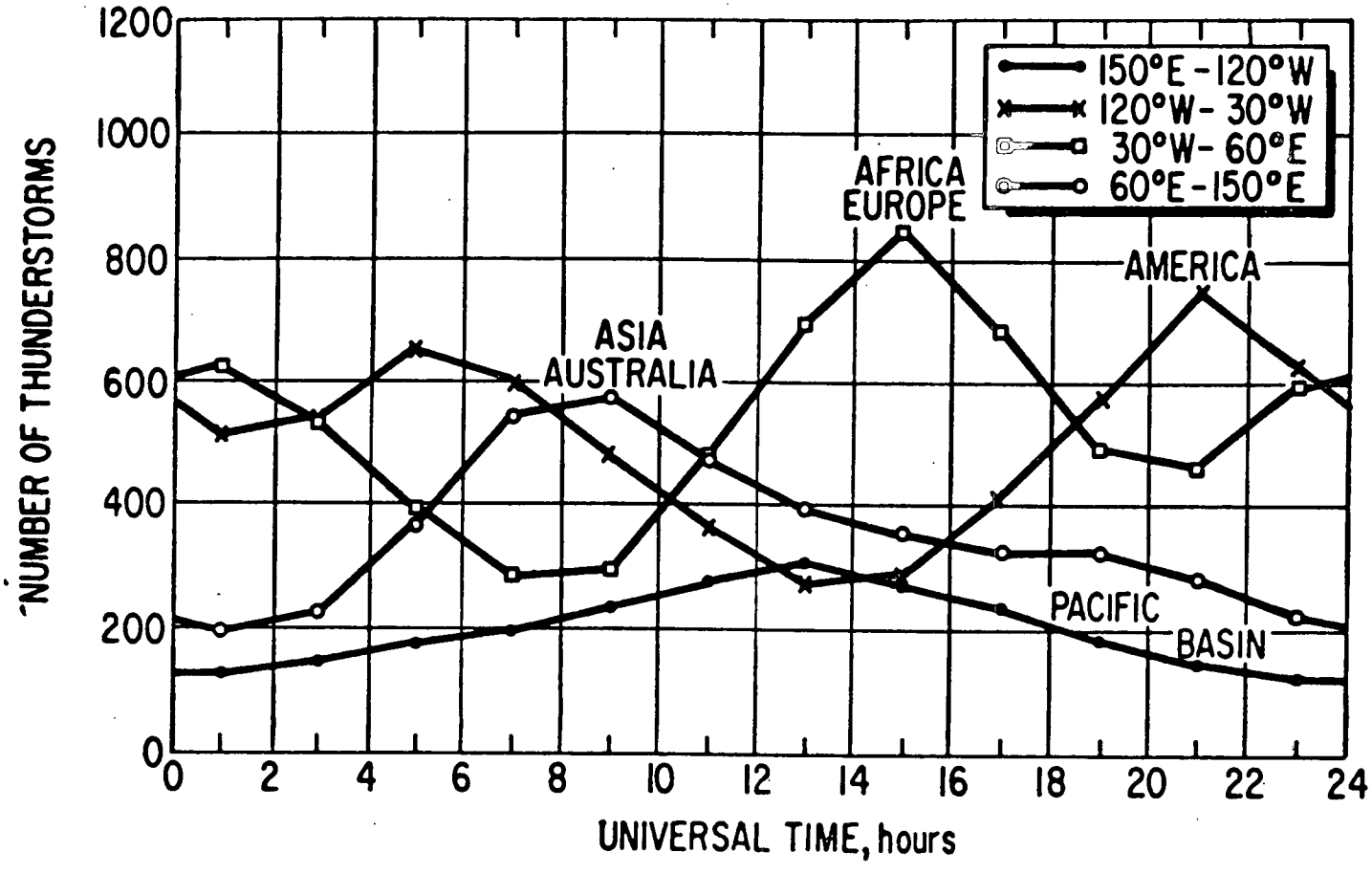

FIGURE 8 - DIURNAL VARIATION IN MEDIAN NUMBER OF THUNDERSTORMS OCCURRING IN THE MAJOR ACTIVE REGIONS FOR SEPTEMBER, OCTOBER, NOVEMBER (AFTER KRUMM, 1962).

for other seasons are similar (see Krumm, 1962), but the continental region having the most storms in progress changes (for example, in July, Asia's is highest) with season. In general, anywhere from about 150 to 1000 thunderstorms will be in progress at any given time depending upon season, time of day and geographic region. No similar diurnal and seasonal statistics exist for ocean regions, but there appear to be far fewer storm occurrences over oceans compared to land masses (Sparrow and Ney, 1971).

Bearing in mind that thunderstorm occurrence varies with time of day and location in a given season and that ionospheric shielding of RAE frequencies also vary in a different way with these parameters, it is instructive to return briefly to Fig 5. Superimposed on the distribution map is a representative RAE orbit beginning at about 1915 UT on the right of the map and terminating at about 2245 UT on the left. Also illustrated are twilight lines separating day from night for two subsolar positions A (at longitude 255° E) and B (225° E). These positions respectively correspond approximately to local noon at the time when RAE crosses the twilight line from post sunrise to night on the Earth below at point A on the orbit, and when it crosses the line again from night to presunset. Because RAE has a component of motion in the same direction as the twilight line, the time period that the satellite is over a darkened portion of Earth is lengthened by about two hours of apparent local time

(30° of longitude) in this particular example, although the real time elapsed is only about 15 minutes.

At the risk of oversimplification, let us assume for the moment that the ionosphere is opaque on the day side and transparent on the night side to illustrate expected effects from the variations in noise source distribution and intensity. After RAE passed point A (Fig. 5) on its orbit it would see a gradually increasing noise intensity as its subsatellite point approached the thunderstorm maximum area north of Australia and a subsequent decrease as it passed over the Indian and South Atlantic Oceans. Then, when it proceeded toward Point B near the South American coast, the noise intensity would again gradually rise, followed by a rapid falloff when point B was traversed. Finally, due to the opacity of the ionosphere, the noise over the Americas would not reach the satellite, even though the transit time coincided with the afternoon maximum in source intensity as is evident in Fig. 7 or 8.

This qualitative picture will be modified by the time and geographic variations of the intervening ionosphere, and moreover, the modification will not be identical on all observing frequencies, due to the frequency dependence of radiowaves passing through the ionosphere. A further complication is the fact that the distributions of thunderstorm activity, even if accurately known are insufficient to describe the distribution of atmospheric radio noise sources viewed by RAE 1.

Radio noise generated by thunderstorms can propagate obliquely to large distances from the source via reflections between the Earth and the ionosphere before reaching a point where its frequency allows it to penetrate through the ionosphere to the satellite. At any given geographic location and time, the noise level at Earth's surface is the sum of contributions from all active thunderstorm regions in the world weighted by the source strengths and propagation loss factors. Two examples of the diurnal variation in total noise power at a fixed location (Kekaha, Hawaii) due to the weighted source contributions are given in Figs. 9 and 10 for Autumn (September, October, November) and Summer (June, July, August), respectively (Herman, 1968). Magnitude of the maximum total is about the same in both seasons, but in Autumn (Fig. 9) the maximum occurs about two hours earlier than in Summer (Fig. 10). The main contributor in Autumn is the America's source with a small contribution from Africa/Europe, and in Summer, Asia/Australia contributes slightly more noise than America with practically no contribution from Europe/Africa.

Using similar concepts, an 18-station network of noise receivers, combined with measurements from C.C.I.R. (1964), has derived the world wide distribution of radio noise as a function of season and time of day. The noise power is expressed in terms of an effective antenna noise factor fâ, defined by

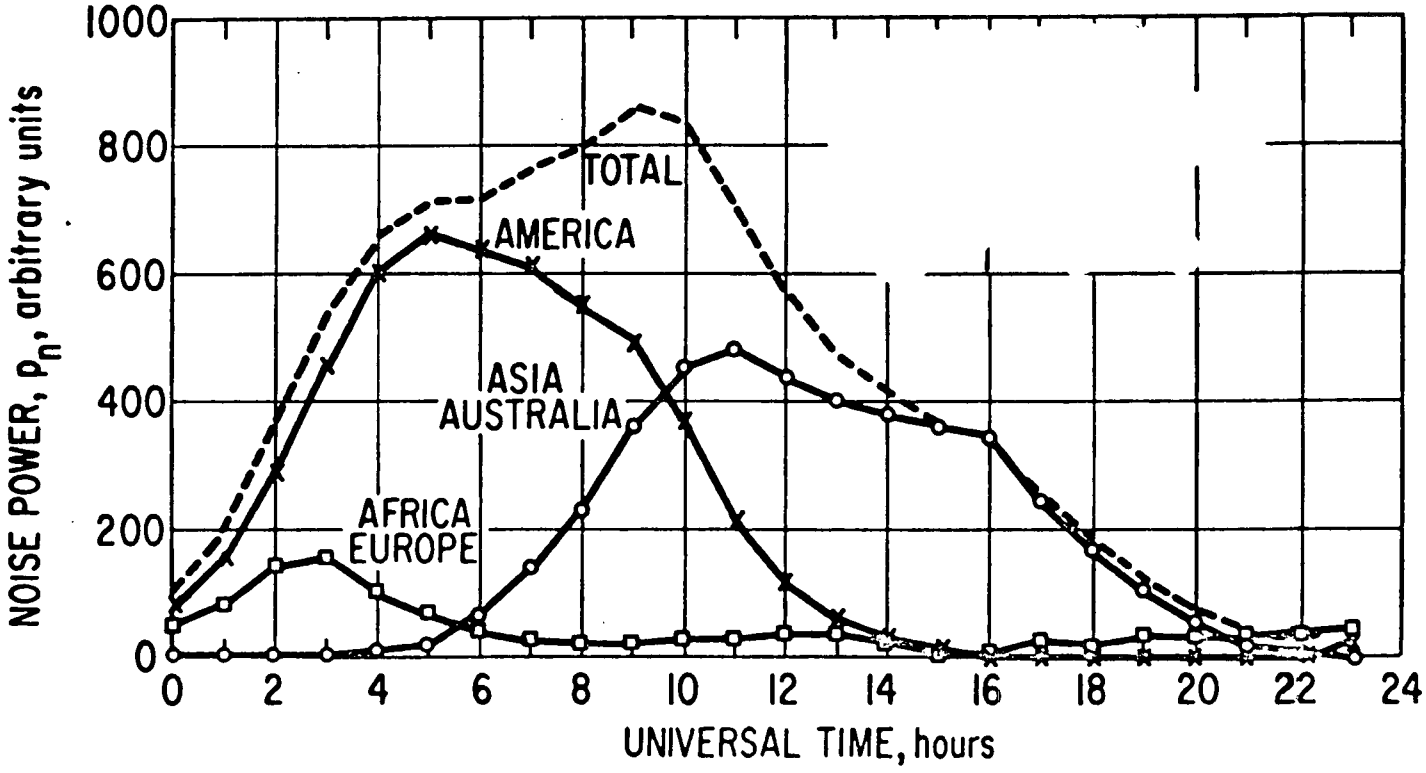

FIGURE 9 - DIURNAL VARIATION IN RELATIVE CONTRIBUTION OF MAJOR THUNDERSTORM AREAS TO THE ATMOSPHERIC NOISE LEVEL AT KEKAHA, HAWAII IN SEPTEMBER, OCTOBER, NOVEMBER (HERMAN, 1968)

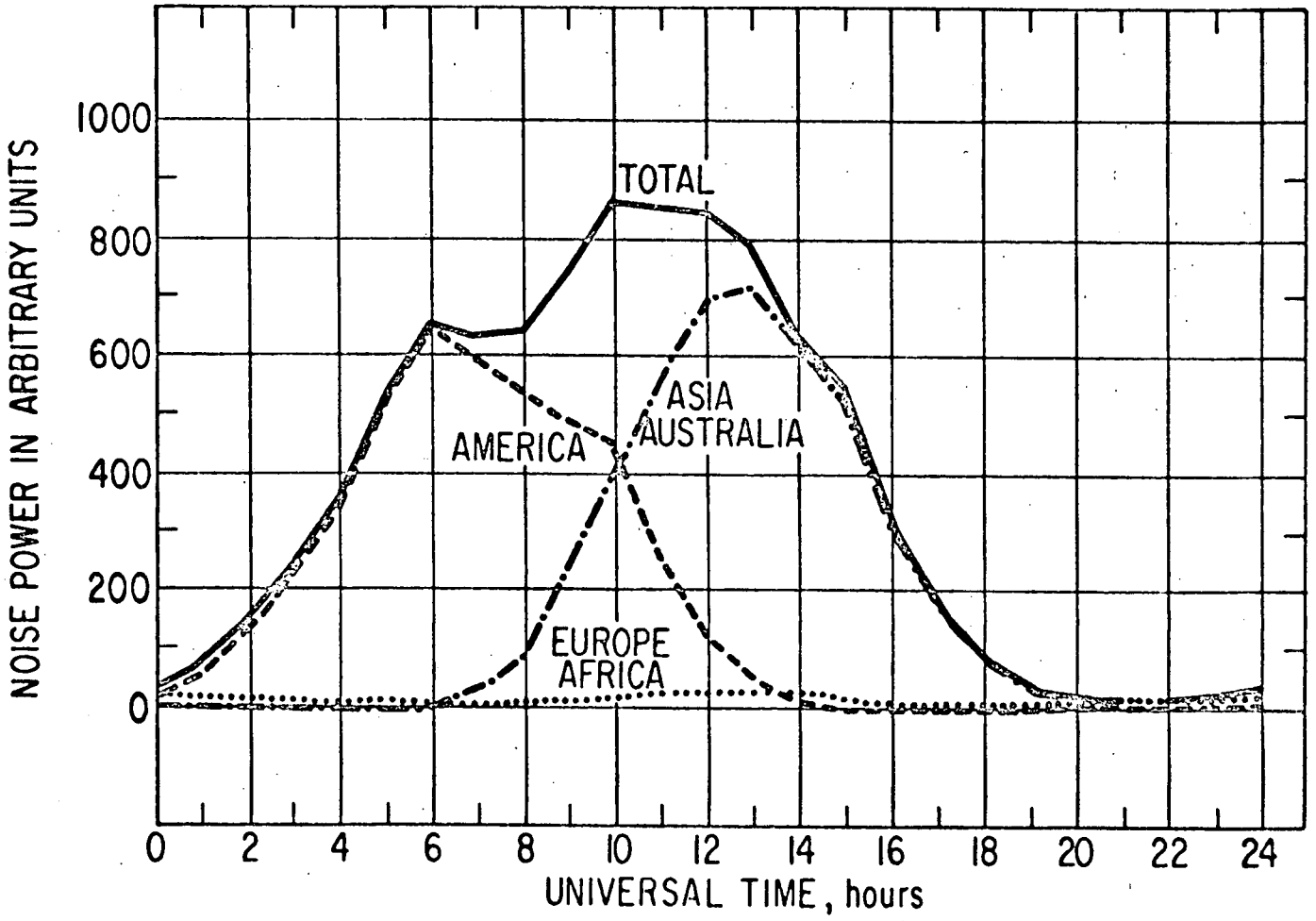

FIGURE 10 - RELATIVE CONTRIBUTION OF MAJOR THUNDERSTORM AREAS TO THE ATMOSPHERIC NOISE LEVEL EXPECTED AT KEKAHA, HAWAII IN JUNE, JULY, AUGUST (HERMAN, 1968).

$$f_a = \frac{p_n}{k\ T_o\ b} = \frac{T_a}{T_o}$$

where

p_n = noise power in watts

k = Boltzmann's constant

T_o = reference temperature = 288° K

b = bandwidth of noise receiver

T_a = effective antenna temperature in the presence of external noise

In decibels (dB), the noise factor is

$$F_a = 10 \log f_a = 10 \log p_n - (10 \log kT_o + 10 \log b)$$

The reference T_o is 288° K to make 10 log kT_o equal to 204 dB below 1 Joule.

The median noise factor in dB for 1 MHz is mapped according to season and 4-hour time block, as illustrated in Figs. 11 and 12 for 0000-0400 LT in Spring (September, October, November in Southern hemisphere) and Summer (December, January, February), respectively. (Graphical conversion factors are provided by CCIR to convert the F_a values to other frequencies). In the illustrated maps it can be seen that the expected atmospheric radio noise level is highest over the continental land masses where thunderstorm activity is high and lowest over the oceans and polar regions. The least noise level is predicted in those regions furthest removed from thunderstorm regions, as would be expected on the basis of the radio propagation and source distribution concepts utilized in the prediction technique.

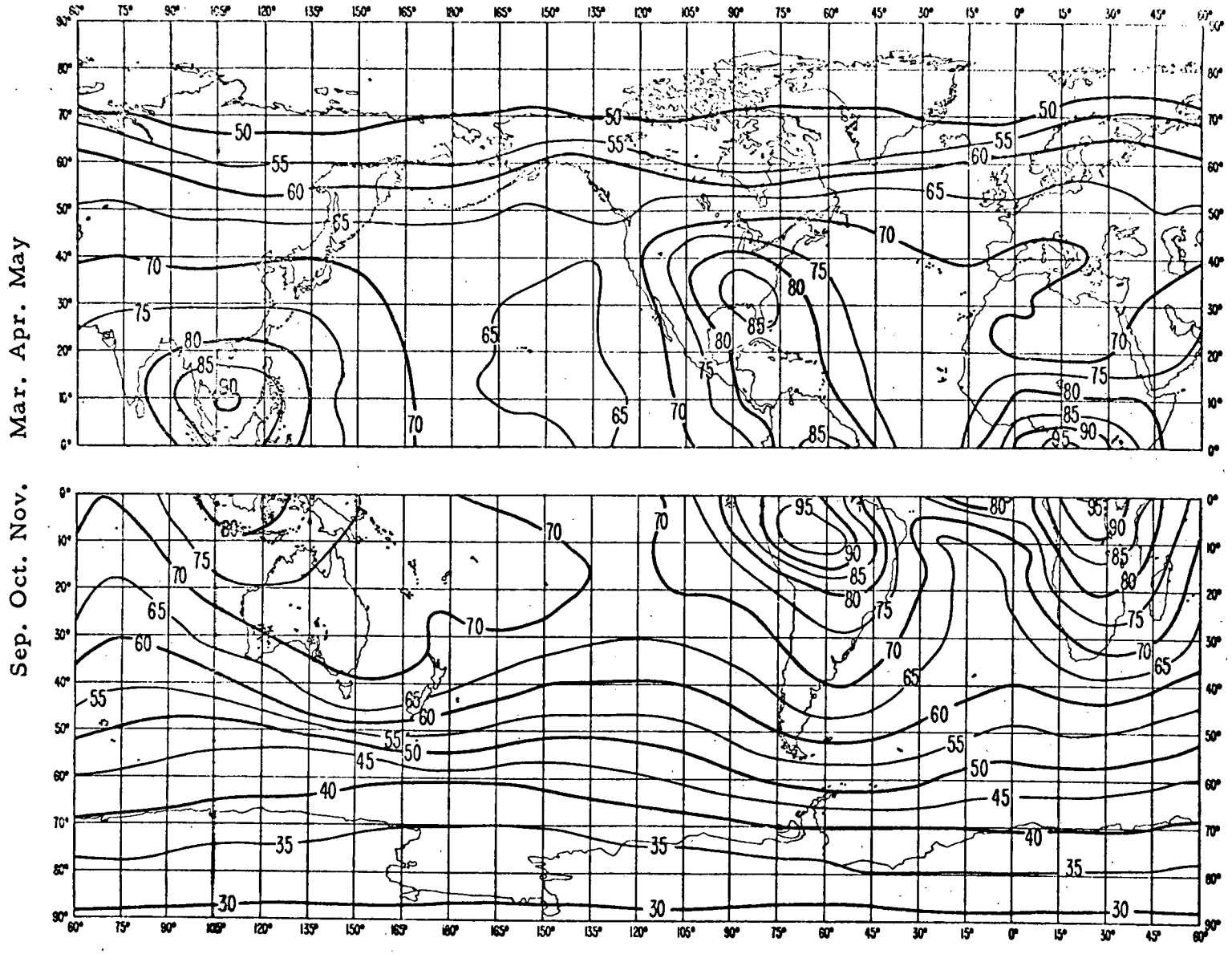

FIGURE 11 - EXPECTED MEDIAN VALUES OF ATMOSPHERIC RADIO NOISE AT 1 MHz IN SPRING, 0000-0400 LT; CONTOURS ARE FAM IN dB ABOVE k T_o b (C.C.I.R., 1964).

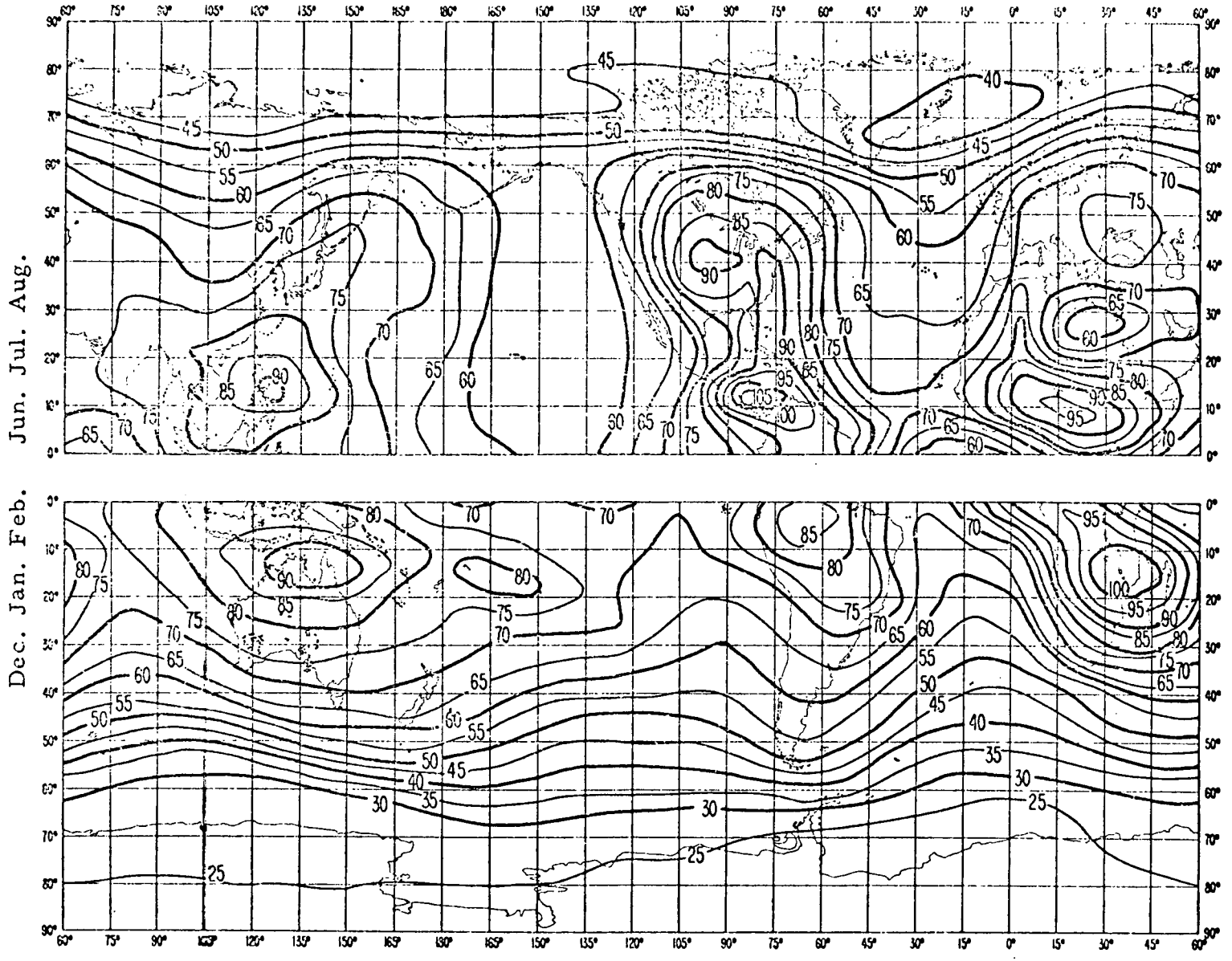

FIGURE 12 - EXPECTED MEDIAN VALUES OF ATMOSPHERIC RADIO NOISE AT 1 MHz IN SUMMER 0000-0040 LT (FAM IN dB ABOVE k T_o b)

Observational noise data useful for correcting the predictions is practically nonexistent for the ocean and polar regions, so the CCIR distributions are least accurate in those areas. It is there that the RAE 1 data are of consummate value. Due to the orbital inclination of the satellite, however, the polar regions cannot be sampled by RAE 1, and the fairly low top frequency (9.18 MHz) precludes observations of terrestrial noise over much of the daylit hemispheres. Despite these limitations, the downward Vee antenna is greatly useful for mapping the noise distribution during darkness between 59° N and 59° S; preliminary maps have been constructed for the southern hemisphere and are discussed in Section 5.

The noise predictions in Figs. 11 and 12 are appropriate for atmospheric radio noise received on an omnidirectional antenna at the Earth's surface. To be seen by RAE 1, the noise arriving at any point on Earth's surface from distant sources has to be scattered upward and outward. Whether or not this upward-scattered component will have an energy flux density comparable to that arriving from all directions, is not known from ground-based measurements, and a theoretical assessment of its possible flux is fraught with difficulties imposed by the numerous assumptions that have to be made. Horner (1965), however, has estimated that

over one of the main thunderstorm areas at 1000 km height and no ionosphere, the power flux density at 10 MHz is 3.9×10^{-17} Wm^{-2} H_z^{-1}. According to Horner (1965) this value is comparable to that near the ground in the main thunderstorm areas. It may be expected then, that synoptic maps of terrestrial noise observed by RAE 1 will have similar patterns if not comparable amplitudes, to the surface maps prepared by CCIR (1964).

It is presently believed that contributions from man-made city noise and radio frequency interference will introduce only second-order effects into the patterns.

4.0 RAE1 NOISE OF TERRESTRIAL ORIGIN

A number of tests based on the concepts discussed in the previous sections have been applied to selected portions of the RAE 1 burst receiver (sweep frequency) and RV (fixed frequency) data on frequencies between 2.7 and 9.2 MHz to determine when and where the measured noise was being received from terrestrial sources below the ionosphere. Noise of magnetospheric origin has been ignored in this part of the analysis (but see Section 6), and galactic noise has been subtracted from the data where appropriate. The tests and their results are presented in this section.

4.1 Sweep Frequency Observations

On the frequencies of interest ionospheric shielding will tend to limit reception of terrestrial noise to periods and locations where foF2 is low; as noted earlier this is generally on the night side. In crossing the twilight transition region from postdawn to predawn, there is a fairly steep negative horizontal gradient in foF2 (see Fig. 1) which would permit the highest frequencies to penetrate to RAE 1 first, followed gradually by the lower frequencies as the satellite crossed the region. Also, the iris effect would allow the highest frequency to be received at the largest slant range. Thus, as RAE 1 crosses morning twilight, the noise level should gradually exceed the cosmic noise background at successively lower frequencies. That this

behavior in fact happens is illustrated in Fig. 13 ; the data presented in this figure is a rather typical example of ground breakthrough.

In Fig.13 contours of measured noise level in dB above cosmic noise background are plotted as a function of frequency and universal time for the period 1006 UT to 1020 UT, December 2, 1968 (Kaiser, 1970). The relevant contours here are between 2.1 and 5.4 MHz. The geographic location of the satellite during this period is shown in Fig. 2, between points A and B. On 5.4 MHz the cosmic noise level begins to be exceeded (Fig. 13), about the time RAE is at A in Fig. 2; by the time it reaches B the noise level on 2.7 MHz is "in" (i.e. has exceeded the cosmic level). The ground range from B to the lowest foF2 region is about 5000 km.

Assuming a constant dB level to represent a threshold level above which the terrestrial noise exceeds the cosmic noise level over the range of frequencies here, it is found that the time required for the noise to break through from 5.4 MHz down to 2.7 MHz is typically about 15 minutes (as it is in the Fig.13 example), and ranges from about 12 to 20 minutes in the 100 odd cases investigated to date.

The ground range from A (where 5.4MHz comes in) to the ground sunrise line (Fig. 2) along the orbit is about 4200 km, and from B (where 2.7 MHz comes in) it is about 1000 km. Considering the iris effect and neglecting refraction, these ranges correspond

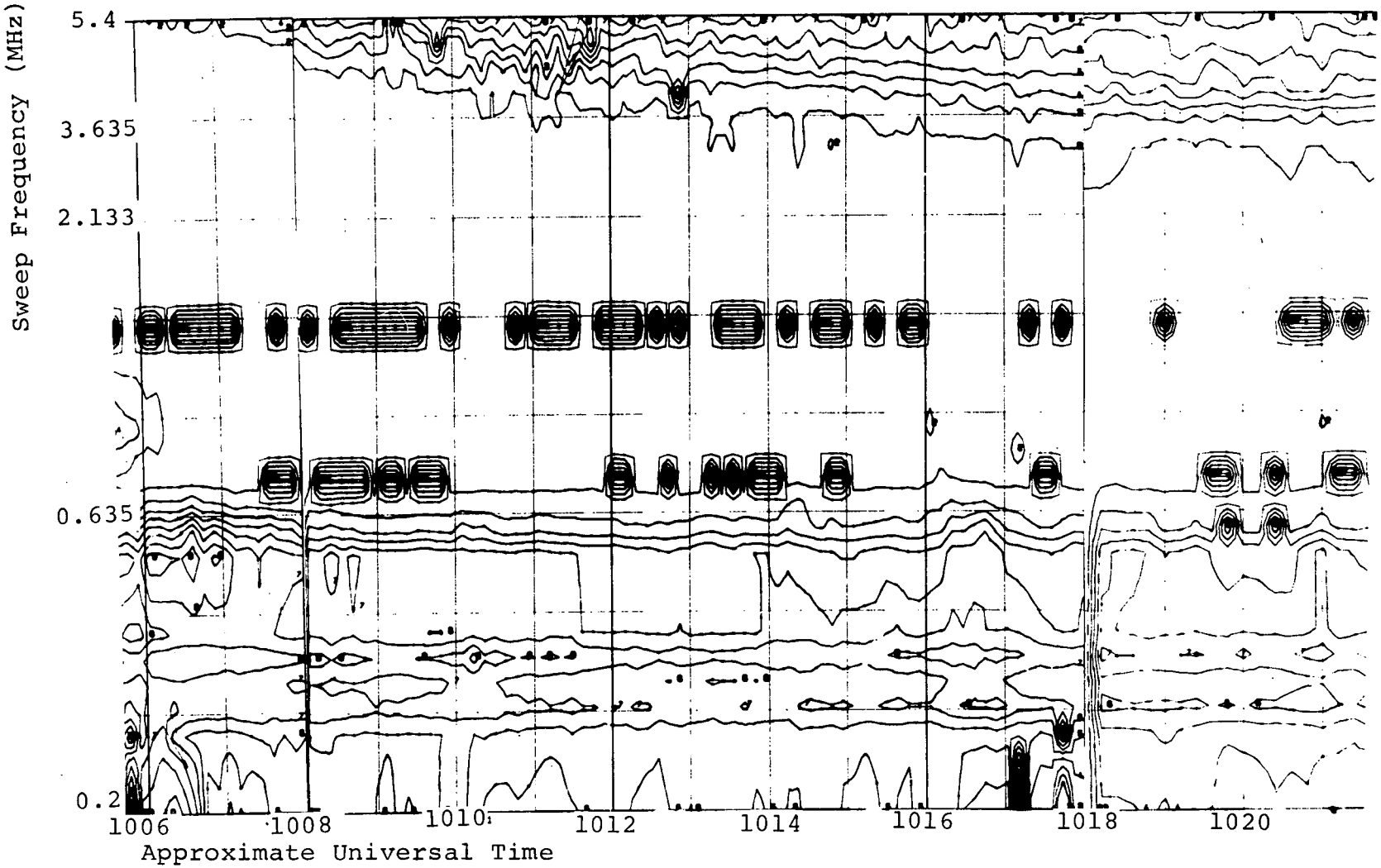

FIGURE 13 - EXAMPLE OF GROUND BREAK-THROUGH IN BURST RECEIVER SWEEP FREQUENCY DATA TAKEN BETWEEN 1006 AND 1022 UT, DECEMBER 2, 1968.

to ratios (foF2/f) of 0.40 and 0.94, respectively (FIG.4). The corresponding critical frequencies computed with 5.4 and 2.7 MHz in the ratio, are agreeably close, being 2.2 and 2.5 MHz respectively. This magnitude (about 2.4 MHz) is less than the predicted foF2 of 4MHz (Fig. 2) but the fact that 2.7 MHz comes in at all is an indication that the predicted value was too high for the specific day in question; and further, the 4 MHz is a minimum foF2 in about the right geographic position.

Following this twilight transition,or ground breakthrough, the noise on 2.7 MHz and above remains in until about 1130 UT, or approximately at point C (Fig. 2) on this orbit; the exact time could not be established due to a missing frame of data.

As a general rule the terrestrial noise disappears in a manner similar to its appearance in the sweep frequency data. That is, the lower frequencies go out first and 5.4 MHz is the last to be seen. The contours thus slope upward (opposite to those in Fig. 13) rather than downward. Again, in general, the shape of the contours in a, shall we say, "ground cessation" period, are less regular than those for morning ground breakthrough; usually because the satellite is traversing the twilight line from the night side to the evening side where the horizontal gradient in foF2 is positive but smaller than it is in the morning. In keeping with this property of the ionosphere, ground cessation usually requires a lengthier period than ground breakthrough.

In the present example, however, cessation takes place at point C (Fig. 2) when the satellite is well into the night side.

Upon inspection of the predicted foF2 contours it is seen that RAE is again passing over a region of expected high foF2 near the equator. Beyond point C along the orbit where foF2 begins to decrease toward higher (southern) latitudes, terrestrial noise is again seen to break through on frequencies above 6 MHz. It was not evident in the BR (sweep frequency) data, but was observed on the RV downward Vee antenna as discussed in the next section.

The relationship of this particular pass to the world-wide distribution of thunderstorms is illustrated in Fig. 6 whereit can be seen that the probability of a thunderstorm being in the neighborhood of the satellite at points A, B, and C is small. The atmospheric radio noise distribution at Earth's surface expected for the period 04 - 08 LT, December, on the other hand, changes by only 5 or 10 dB as RAE 1 proceeds from point A to point C (Fig. 14). From this it appears that in the present example, ground breakthrough and cessation are dictated more by ionospheric effects than by terrestrial noise variations.

Other ground breakthrough examples in the BR data are amenable to analysis in the same detail as above. However, the ionospheric effects tend to dominate because the amplitudes of the terrestrial noise are difficult to derive from the data. Variations of RAE noise amplitudes due to variations in terrestrial noise distributions are better determined from the

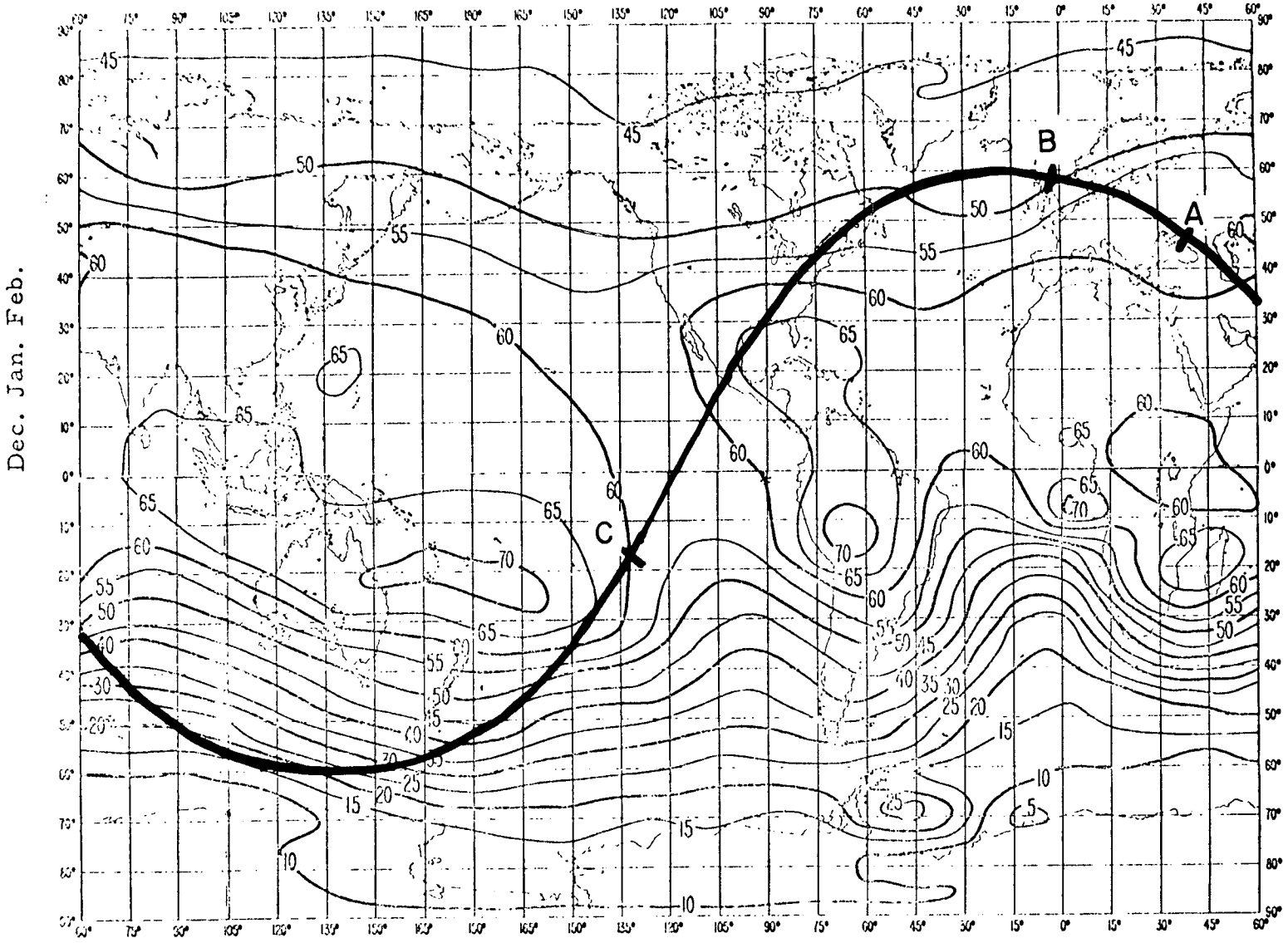

FIGURE 14 - EXPECTED DISTRIBUTION OF ATMOSPHERIC RADIO NOISE ON 1 MHz (IN dB ABOVE k T_o b) FOR DECEMBER, JANUARY, FEBRUARY, 0400-0800 LT (AFTER C.C.I.R., 1964). THE RAE ORBIT CORRESPONDS TO THE ONE IN FIGS. 2 AND 6

fixed frequency RV receivers on the downward Vee antenna. A discussion of the RV observations on specific RAE passes is given below, and geographic distributions of terrestrial noise derived from a series of consecutive passes are discussed in Section 5.

4.2 Terrestrial Noise on the Downward Vee-Antenna

Analysis of the data from the downward Vee antenna in the frequency range from 3.9 MHz to 9.2 MHz displays a marked frequency dependence of onset and termination times. A typical example is shown in Figures 15 and 16. Figure 15 represents a full orbit of data for December 2, 1968, between 0008 UT and 0350 UT for an observing frequency of 9.180 MHz. The upward Vee antenna is directed toward the North Galactic Pole while the downward Vee antenna is directed toward the Earth. The front/back ratio at 9.180 MHz is 13 dB. The dipole antenna is effectively directed toward both the North Galactic Pole and the Earth. Looking at the peak noise temperature on the downward Vee antenna, one can read a temperature of at least 10^{10}°K. In this particular example the receiver has been saturated. Under these circumstances the data point is plotted at a value of 10^{10}°K. The value of noise temperature taken at the corresponding time on the upward Vee has a value of 2×10^{9}°K. This results in a difference in receiver noise power of 10 dB or more and it seems clear that the noise source is located below the satellite. Again, looking at the lower V, onset time on 9.180 MHz occurs at 0230 UT. The sub-

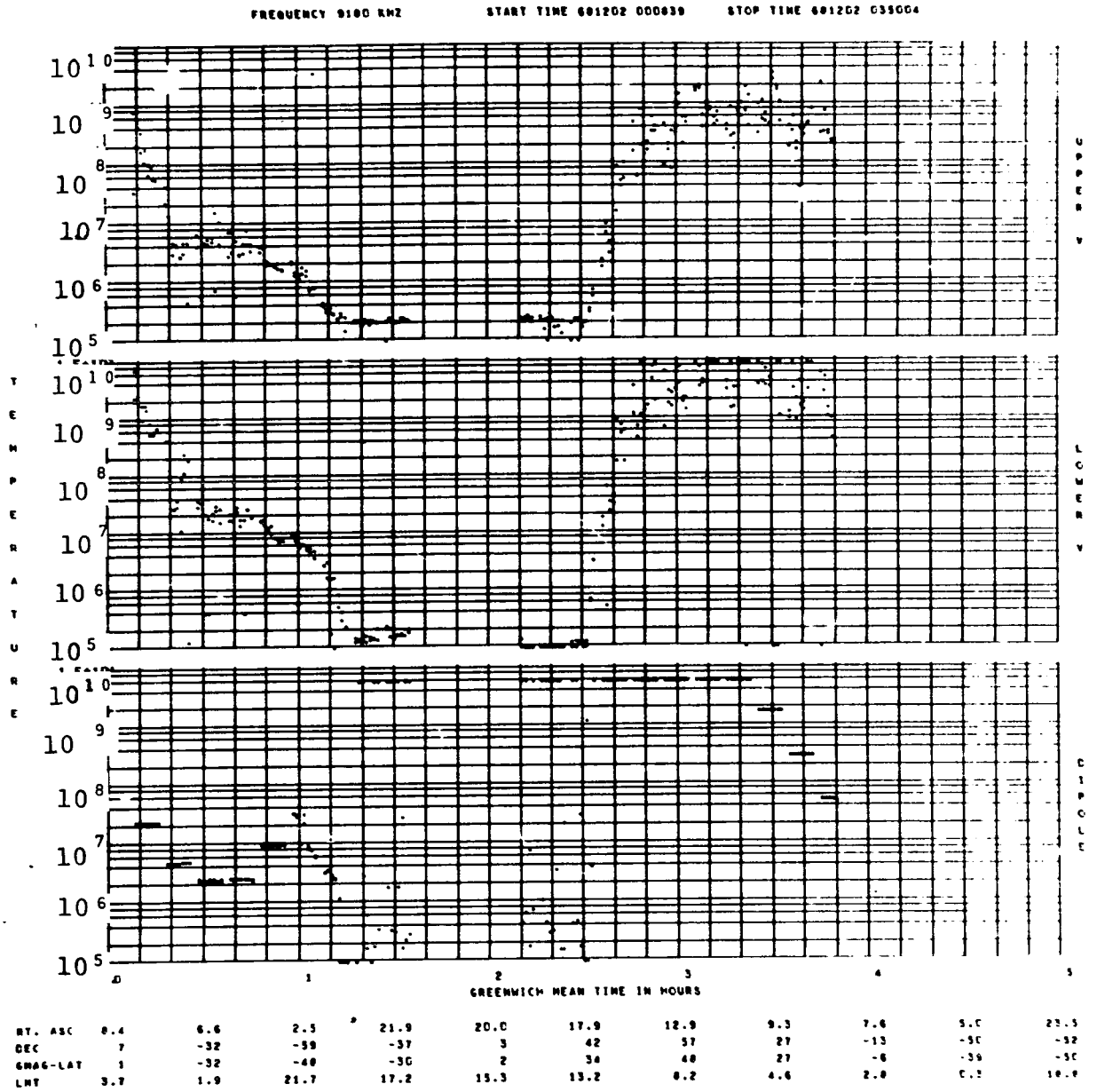

FIGURE 15 - REPRESENTATIVE RV DATA DISPLAY SHOWING A FULL ORBIT OF DATA ON THE UPPER AND LOWER VEE'S AND THE DIPOLE ANTENNA. NOISE TEMPERATURE IS PLOTTED AS A FUNCTION OF UNIVERSAL TIME.

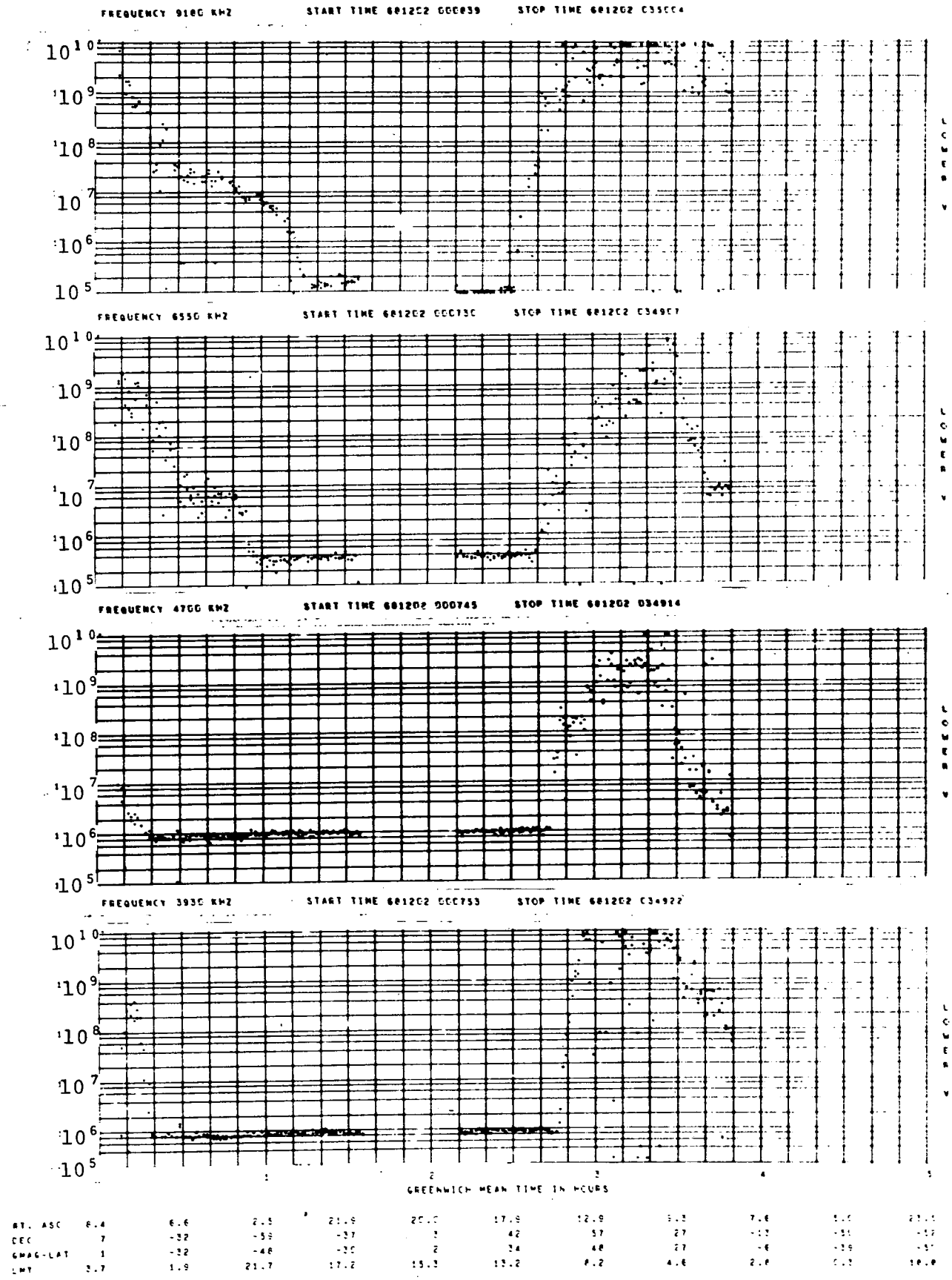

FIGURE 16 - COMPOSITE GRAPH OF FULL ORBIT LOWER VEE ANTENNA DATA ON 3.9 MHz, 4.7 MHz, 6.55 MHz and 9.18 MHz EXHIBITING VARIATION IN ONSET TIME AS A FUNCTION OF FREQUENCY.

satellite point is on the night side of its orbit at 0234 local time.Figure 16is a display of the four frequencies examined, 3.93 MHz,4.7MHz,6.55 MHz,and 9.18MHz,with only the lower Vee shown. Onset time on 6.55MHz,occurs at 0240 UT,4.7 MHz at 0253 UT, and 3.93 MHz at 0257 UT with corresponding local times ranging from 0128 LT to 2338 LT. The onset times for the 4 frequencies occur in descending order on the night side of the orbit as the satellite traverses a region of descending critical frequency. The time interval between onset time on 9.18MHz and 3.93MHz is 27 minutes. The amplitude on each frequency increases to some maximum value and falls off as the satellite moves into the day side.

Figure 17 is representative of the sequence of termination times as the satellite moves into the day side. 3.9 MHz terminates at 1505 UT, followed by 4.7MHz at 1510 UT, 6.55 MHz at 1520 UT, and 9.18MHz sometime after 1520 UT. Again, the onset times occur in descending order starting with the highest frequency. Looking at figure 18 , the satellite is entering a region of descending critical frequency with the 3.9MHz signal reaching maximum noise power at point E which corresponds to a region with a critical frequency of approximately 3 MHz.

Referring again to Figure 17 , at approximately 1215 UT, the satellite is receiving a strong signal on both 9.180MHz and 6.55MHz. On all frequencies below 6.55MHz the ambient background noise is observed. The location of the orbit is plotted in Figure18 . Point D on the plot corresponds to 1215 UT, the time at which

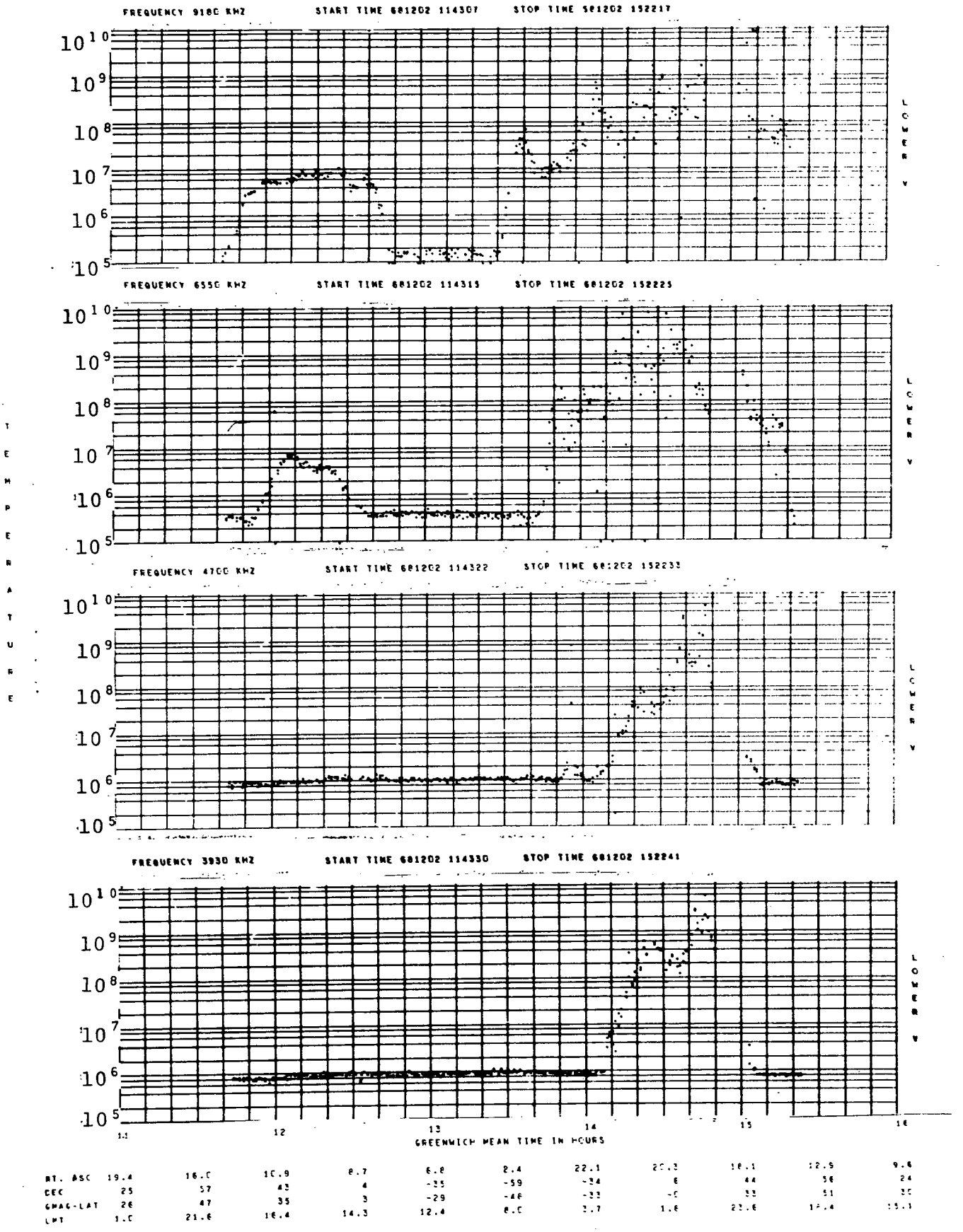

FIGURE 17 - COMPOSITE GRAPH OF FULL ORBIT DATA SHOWING BOTH ONSET TIME AND TERMINATION TIME AS A FUNCTION OF FREQUENCY.

maximum noise power is received on 9.2 MHz and 6.55 MHz. The critical frequency in this region is approximately 6.5 MHz. Consequently, frequencies below 6.5MHz would not be expected to penetrate the ionospheric layer. By the same token, it is quite reasonable to expect frequencies equal to or greater than 6.5MHz to penetrate the ionosphere. An additional point of interest should be mentioned with regard to the equivalence of the ambient noise level on both the upper and lower Vee antenna for the particular frequency being investigated. The ambient noise temperature cannot be measured when the satellite orbit is on the day side of the ionosphere. In this case, the ionosphere effectively shields the satellite from terrestrial noise sources radiating at the frequencies of interest. Consequently the ambient received noise power has its origin in non-terrestrial sources. The primary contribution to the noise power under the prevailing conditions is cosmic radiation. The characteristics of both the upper and lower Vee are identical except for physical orientation. Physically the Vee antennas are mirror images pointing toward both the north galactic pole and the center of the Earth.

The main beam of the upper V sees the incident cosmic radiation while its back lobe sees the same radiation after reflection from the topside of the ionosphere. The critical frequency of the ionosphere is such that radiation on the frequencies under consideration suffer specular reflection after impinging on the ionosphere. Thus the ALBEDO is essentially

equal to one. The back lobe of the lower Vee antenna sees the incident radiation while the main lobe receives the reflected radiation. Because of the essentially non-dissipating reflection, and the identical antenna patterns, the received power on both upper and lower Vee antennas are equivalent. The ambient noise power on the dipole antenna is slightly higher than the Vee antenna as would be expected due to the higher integrated flux density received.

Very strong evidence to further substantiate the contention that the noise power is of terrestrial origin is furnished, if one examines the relationship between the change in critical frequency as a function of the trajectory of the sub-satellite point during the period of ground breakthrough, and the time elapsed between onset times on 9.2 MHz and 2.7 MHz. Again, taking Fig. 17 as an example, the difference in onset times between 9.2 MHz and 2.7 MHz is 37 minutes. This represents a distance of approximately 6300 km along which the sub-satellite point has moved.

From Fig. 18 the distance between the values of a critical frequency of 9 MHz and 3 MHz along the projected satellite path can, in this case, be calculated easily with a fair degree of accuracy. The projected satellite path traverses approximately 70° of longitude at an average latitude of 52° North. The resulting distance is approximately given by

distance = (111) x degrees of longitude x COS (lat)

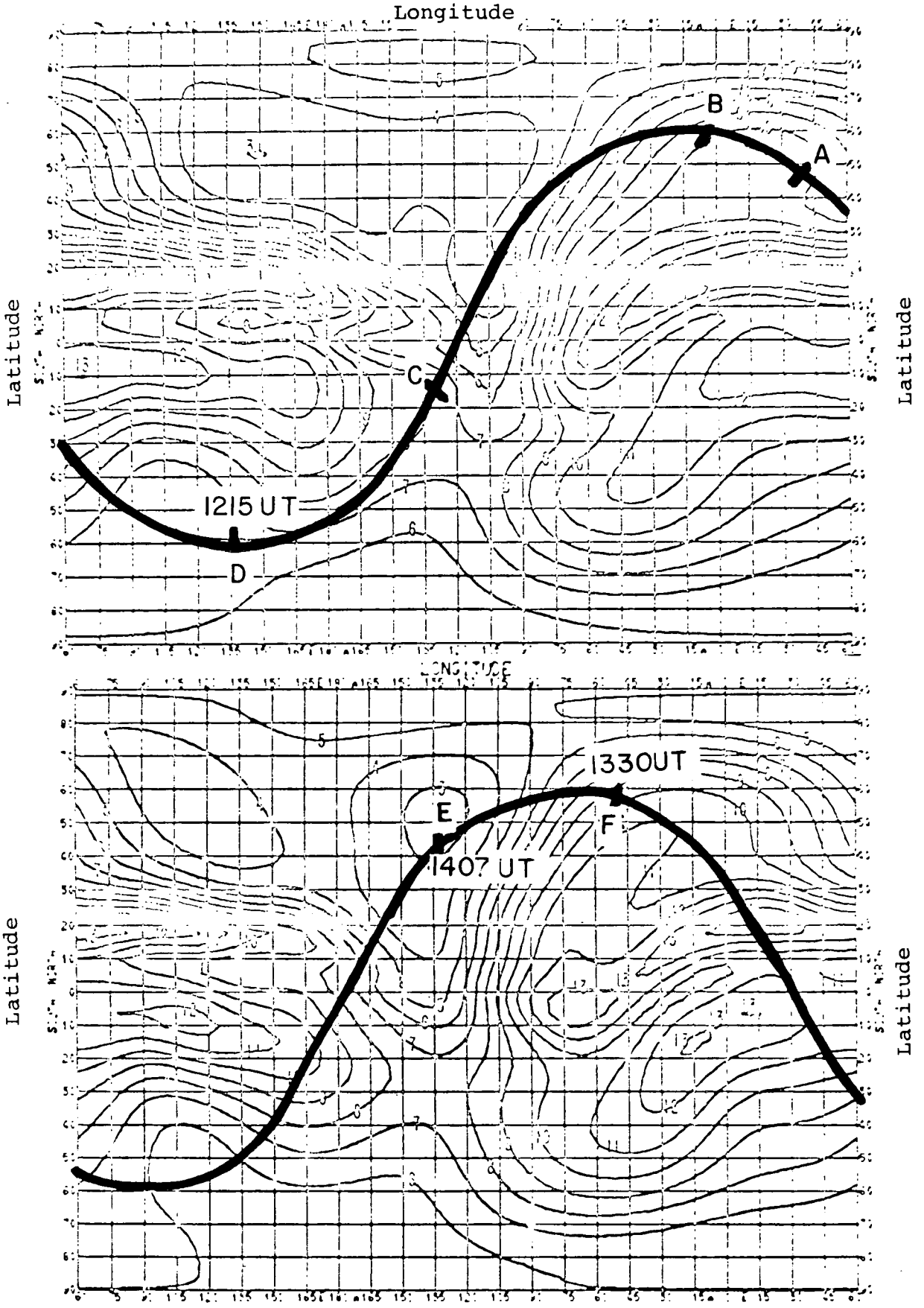

FIGURE 18 - PLOT OF TWO CONSECUTIVE ORBITS SUPERIMPOSED ON PREDICTED foF2 CONTOURS FOR DECEMBER 1968 AT 1200 UT AND 1400 UT.

The result is a distance of 6150 km which agrees very well with the value of 6300 km calculated above on the basis of measured onset time difference.

Both of the above distances are in good agreement with the distance obtained from the curve of foF2/f vs. ground range shown in Fig. 4. With a critical frequency of 2.7 MHz and an observed frequency of 9.2 MHz a ground range of 6450 km is obtained. The three independent distance measurements show a maximum deviation of 4.5%. Since distance is proportional to time, there exists very good correlation between experimentally measured onset time differences and calculations of onset time differences on the basis of ionospheric characteristics and propagation effects.

To summarize then, the Earth's surface can be thought of as radiating on at least all frequencies observed by the satellite with the ionosphere acting as a shield whose opacity is a function of frequency. In the example described, the earliest time at which the satellite "sees" 9.2 MHz is that time at which the sub-satellite point crosses the 9 MHz critical frequency contour. It continues to receive the 9 MHz signal until the satellite moves into a region where the critical frequency exceeds approximately 9 MHz. As the satellite moves into a region of decreasing critical frequency moving toward the 3 MHz contour it continues to receive signal on 9 MHz. The same phenomenon occurs on the lower frequencies for appropriate critical frequencies.

It is of considerable importance to determine noise power from terrestrial sources as a function of frequency. Because of the difficulty involved in the differentiation between the contributions of each of the variable sources to the total power, no attempt has been made in this study to separate out individual power components. However, the reduction of total power into individual source contributions should be done in the future . An attempt has been made to deduce the frequency-dependence of the composite terrestrial noise at RAE 1. The data sample consisted of 40 data points on each frequency taken at peak noise temperature. The values were averaged and a graph of noise temperature as a function of frequency was generated. This graph is displayed as the uppermost curve in Fig. 19.

This curve represents the total power received at the satellite. In order to look at the noise temperature resulting only from terrestrial sources the received cosmic noise power must be subtracted from the total power. Stone, (1969 and references therein), has shown that the cosmic noise power peaks at 3 MHz and falls off as $1/f^{2.2}$ with increasing frequency. Converting Stone's value of brightness at 3 MHz to temperature, the following expression for the noise temperature results:

$$T_{cosmic} = 3 \times 10^8 / f^{2.2}$$

The values of T cosmic as a function of frequency are plotted as the lowest curve in Fig. 19. The remaining curve, is the total noise power minus the cosmic noise power. As can be seen from the figure:

$$\frac{P_{cosmic}}{P_{total}} << 1$$

and cosmic noise has a negligibily small effect on both the amplitude and shape of the total power curve. The most striking feature of the resulting power curve is the presence of a minimum at approximately 5.5 MHz. In order to account for the minimum on a theoretical basis, a simplified propagation model was employed as a first approximation. Aiya (1955) has derived a theoretical formula which states that the atmospheric noise power is inversely proportional to the square of the frequency.

Taking into account only the loss due to attenuation, the exponential law of absorption of Bougoir and Lambert (Lipson and Lipson, 1969) can be used to give

$$P_{satellite} = P_{radiated} \exp [-K(f)X]$$

Making use of Aiya's (1955) formula for $P_{radiated}$ and taking the absorption coefficient K as inversely proportional to the square of the frequency one obtains:

$$P_{sat} = \frac{A}{f^2} \exp (-B/f^2)$$

The resulting function for the received power contrary to the observed results, has a maximum rather than a minimum at $f = \sqrt{B}$. This indicates that the model described above is oversimplified

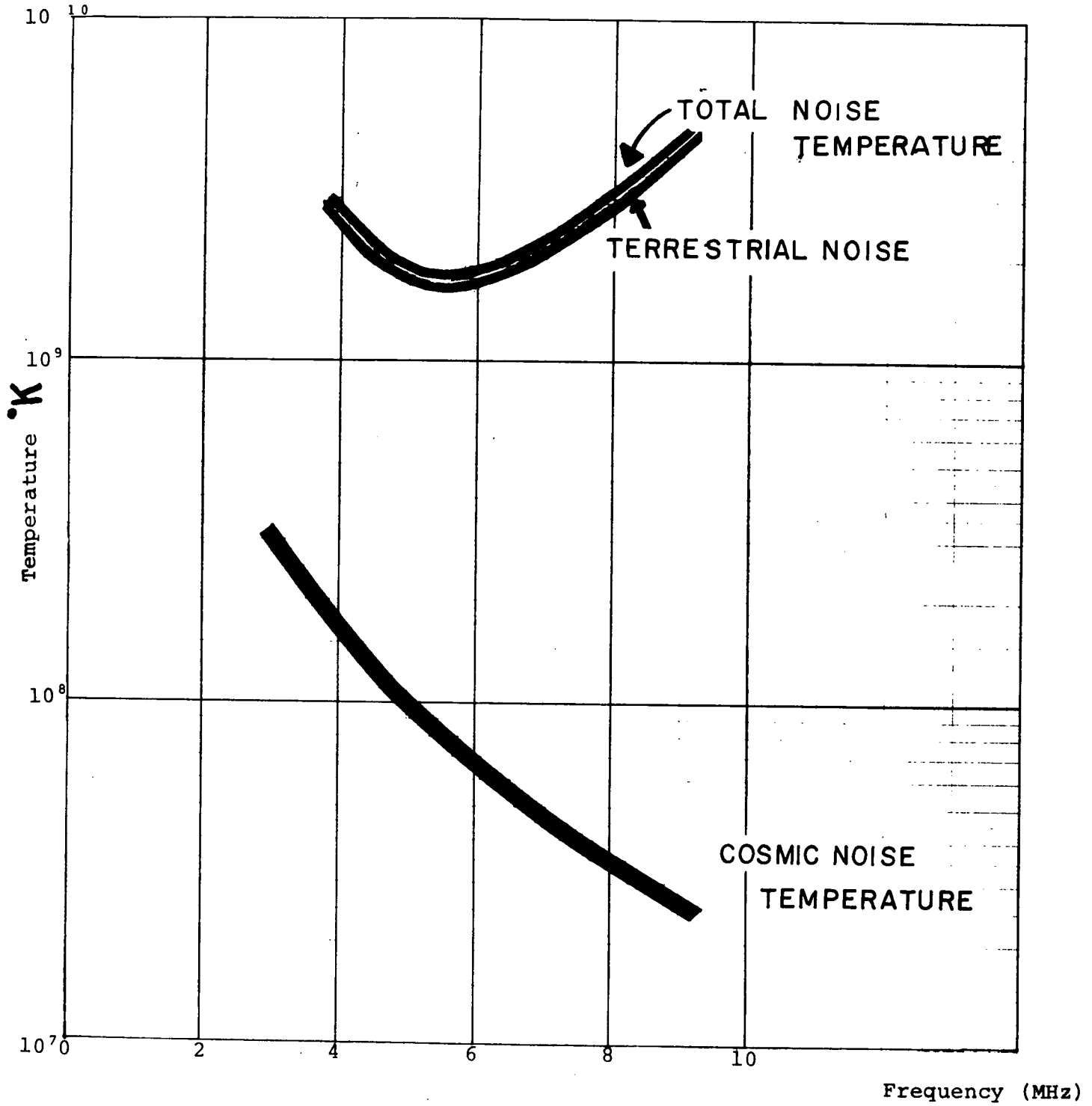

FIGURE 19 - TOTAL NOISE TEMPERATURE AND NOISE TEMPERATURE DUE TO TERRESTRIAL SOURCES AS A FUNCTION OF FREQUENCY.

and that factors such as the extent of the source, the antenna beamwidth, the size of the iris, refractive effects and scattering cannot be neglected. A more sophisticated theoretical model incorporating the neglected factors may very well account for the observed minimum. For example, considering that the received power would be the total integrated power over the area of the effective iris, one would expect an increase with increasing frequency above some minimum because the iris area, as shown earlier, is directly proportional to the observing frequency. Future studies should further investigate the nature of the theoretical power curve in order to more fully explain the results of the experimentally observed power curve.

It has been emphasized earlier that electric discharges due to thunderstorm activity comprise the major source of terrestrial noise power as seen by the satellite. It would be quite desirable to be able to resolve individual storm centers and to obtain information regarding the extent of the storm area, its duration and the power radiated by the storm area as a function of frequency. There are a number of difficulties involved, principally those relating to the large surface area from which the satellite antenna can receive radiation. A preliminary application of the RAE I data to this question has been made, as discussed below. It must be emphasized, however, that these results are only tentative.

The primary geographic locations studied were equatorial land areas where thunderstorms can be regarded as occurring regularly from day to day. Storms at higher latitudes are

more sporadic. Attention was focused on the frequency 9.2 MHz where the critical frequency is low enough on the night side so that refractive and attenuative effects of the ionosphere are negligible. The power flux radiated in a vertical direction from a thunderstorm area may be calculated by (Horner, 1965):

$$\text{Vertical Power Flux} = 100\Pi\, JN\, (1/4 - 1/4 \cos 2\phi - LN \cos\phi)\ \frac{W}{m^2}$$

where J = Energy flux in Joules/m^2

N = Rate of discharge occurrence in km^{-2} sec^{-1}

and TAN ϕ = R/h

where R = Radius of the storm area in km

h = Height of the satellite in km when the satellite is directly overhead

If we assume a value of $N = 10^{-5}$ km^{-2} sec^{-1} and following Horner(1965), a value of $J=2.1 \times 10^{-14}$ Joules/m^2 at 10 MHz in a bandwidth of 1 KHz, with circular thunderstorm of 1000 km radius the calculated power flux at 6000 km altitude would be 1.4×10^{-17} W/m^2.

Taking into account the bandwidth and antenna aperture of RAE I for 9.2 MHz, this amount of power flux would yield a measured temperature of about 10^{15}°K which would be a maximum attained only when the antenna beamwidth encompasses the whole thunderstorm area. The RV receiver saturates at 10^{10}°K, so it is not possible to verify Horner's prediction with the present data.

It is possible, however to estimate the approximate size of a thunderstorm area from the data as follows:

Based on the storm model and the calculations above one would expect the signal level to increase as the satellite approaches the storm area, peaking when the whole storm area is encompassed by the projected area of the antenna beamwidth and falling off as the satellite moves away assuming the storm area is moving very slowly relative to the satellite. If the circular storm area has a diameter of 2000 km, a first approximation to the width of the enhanced signal level due to radiation from the storm area can be made by employing the motion of the projected antenna pattern along the earth's surface. That is,the distance over which RAE I views the storm is the sum of the thunderstorm diameter and projected major axis of the antenna on the surface. Taking the case of the satellite passing directly over the storm center,the sub-satellite point should traverse a distance of approximately 3400 km. The satellite velocity is 5.68 km/sec. The time elapsed (t) during the 3400 km movement of the sub-satellite point is given by

$$t = \frac{2R}{60V} = \frac{R}{30V} \quad \text{(min)}$$

where V = satellite speed (km/sec)

R = sub-satellite distance (km)

The calculated time interval is approximately 20 minutes.

An example of what appears to be power radiated from two discrete thunderstorm centers located over the East Indies and over Australia is shown in Figures 20 and 21. The observing frequency is 9.180 MHz. The basic features of the curve in figure 20 show two discrete peaks with noise temperatures of 2×10^{9}°K and 10^{10}°K respectively. The width of the first peak which occurs in the vicinity of Borneo is approximately 20 minutes which corresponds favorably with the width calculated above. The width of the second peak is about 30 minutes long. The most immediate explanation for the larger width is that the second storm covers a larger area, the higher maximum noise temperature being a result of an increase in the rate of discharge N (i.e. a more intense storm).

The example presented above is seen to recur throughout the data, so further study in this area should be pursued in order to test these tentative results.

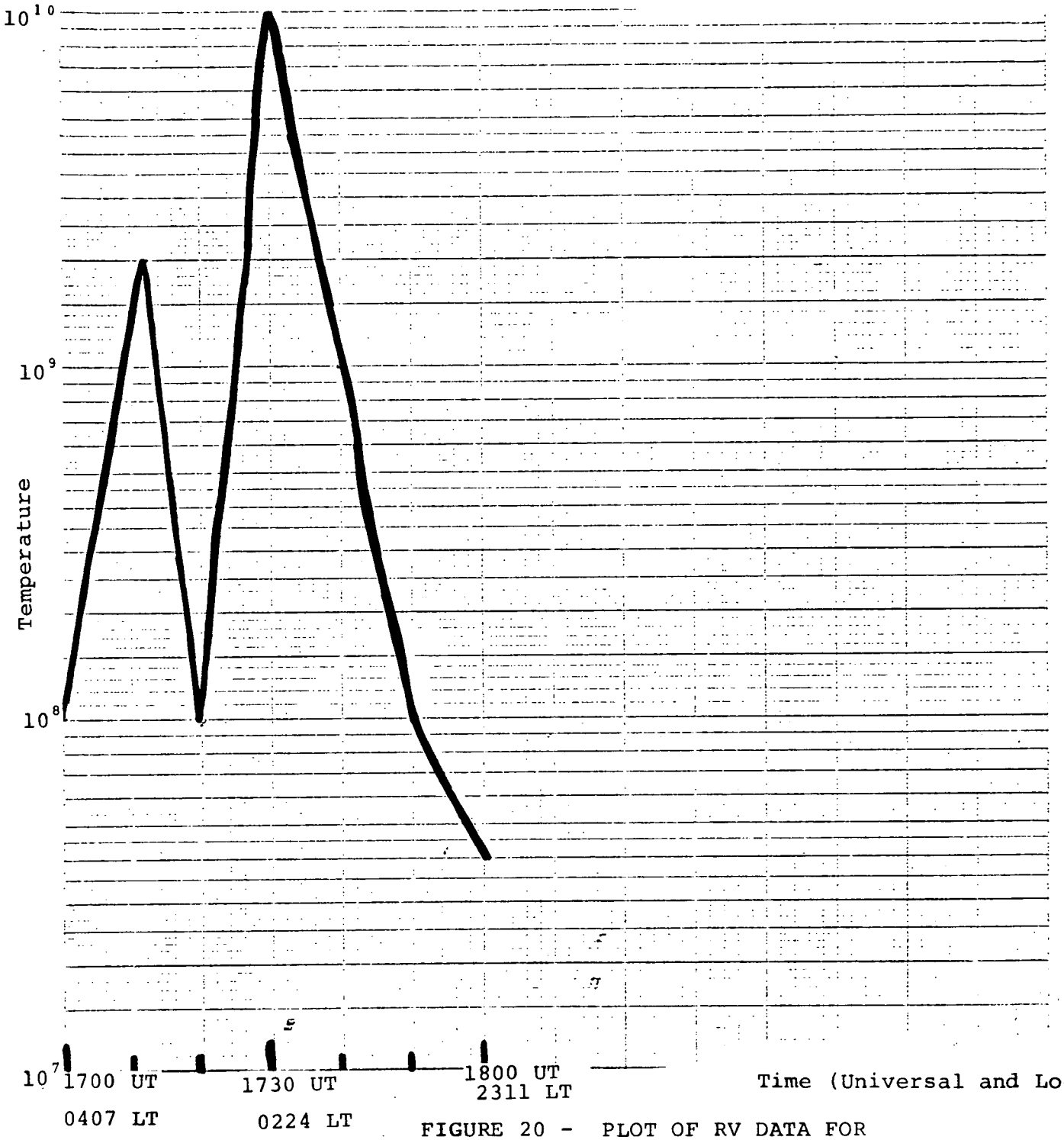

FIGURE 20 - PLOT OF RV DATA FOR 9.18 MHz DURING A PERIOD OF THUNDERSTORM ACTIVITY OVER THE EAST INDIES AND THE AUSTRALIAN CONTINENT.

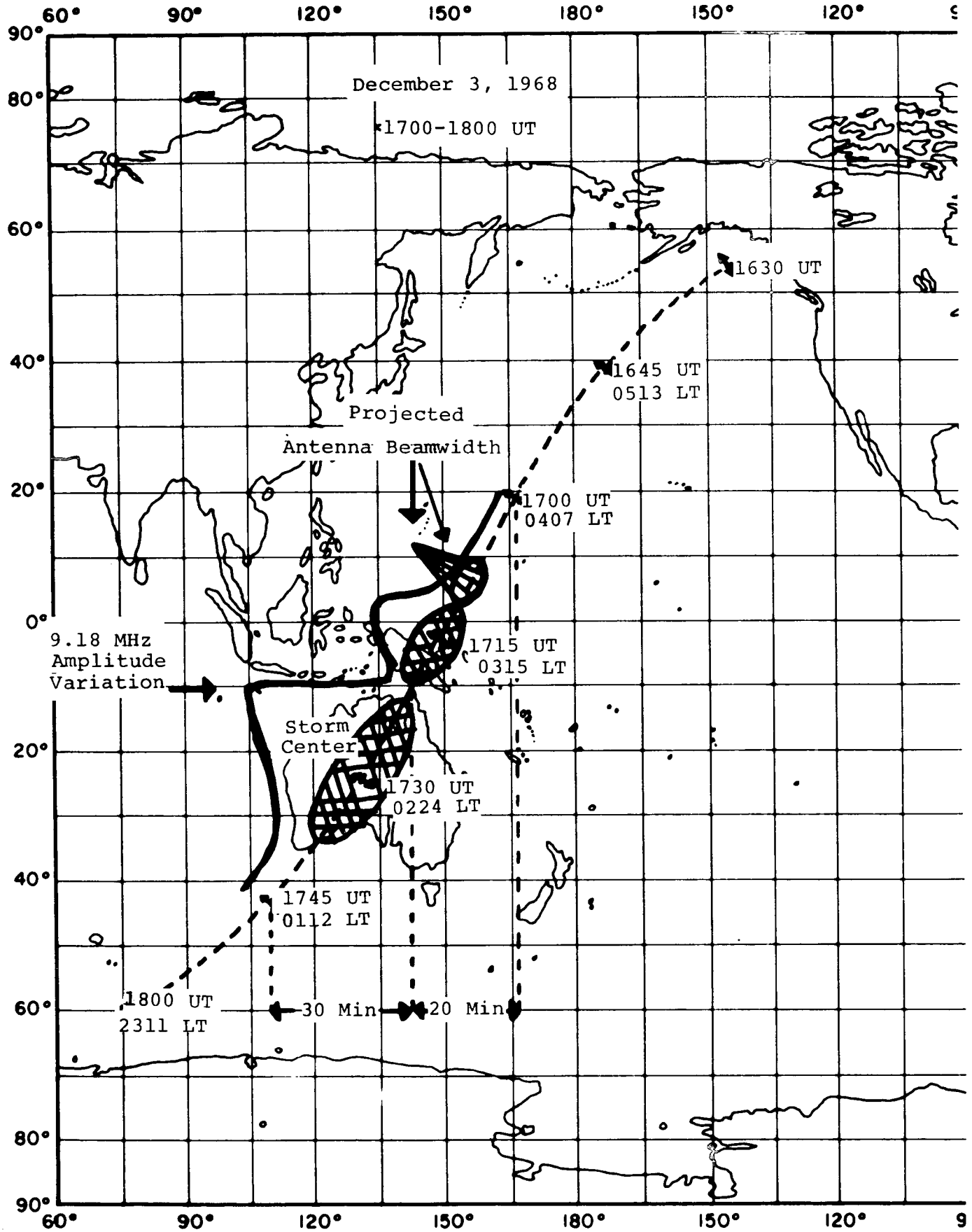

FIGURE 21 - A DISPLAY OF SATELLITE PATH AND NOISE TEMPERATURE VARIATION ON 9.18 MHz AS THE SATELLITE PASSES OVER THUNDERSTORM CENTERS OVER BORNEO AND AUSTRALIA

5.0 DISTRIBUTION OF TERRESTRIAL RADIO NOISE

5.1 Method of Analysis

Having demonstrated that the night time noise measured on the downward Vee antenna is principally of terrestrial origin, we are now in a position to deduce its spatial distribution over the Earth's surface. As a first approach, part of the RV data on 9.18 MHz has been analyzed for this purpose.

Selection of the data points was made by restricting the time of interest to the local time (LT) hours between 00 and 04 LT. For the periods October 15-22, 1968 and December 2-6, 1968, all times within 00-04 LT appearing in the 15-minute UT emphemeris were used to determine the satellite position (geographic latitude and longitude) along with the appropriate universal time. Then, using the UT times to enter the RV (whole orbit) data, the noise magnitude for 9.18 MHz on the downward Vee was established, and converted to dB above 288°K. This reference termperature agrees with that utilized by C.C.I.R so that a direct comparison can be made between the RAE measurements and CCIR predictions.

These dB values were plotted at their corresponding geographic positions on base maps drawn in modified cylindrical projection. Isocontours of dB levels at 5 dB increments were then manually constructed through the data points. Some smoothing was necessary to maintain continuity in the contours, and there is, of course, a degree of "geophysistic" (analogous

to "artistic") license in their construction. This license is justified in part on the basis of known variations in terrestrial noise level observed by ground-based techniques and ionospheric propagation at HF. It is further justified by the results, which show that, with only one or two exceptions, all data points lying between two adjacent contours have magnitudes within the 5-dB interval defined by the two contours and are approximately linearly proportional to their distance from the lines.

Two preliminary maps constructed by this technique are illustrated in Figs. 22 and 23, for October 1968 and December 1968, respectively. These maps have several limitations, as discussed in the next section.

5.2 Results

The maps illustrated in Figs. 22 and 23 cover only the sourthern hemisphere due to the selection of input data only for 00-04 LT. Full coverage "night time" maps can be gained from utilizing data for the time blocks 20-24 LT and 04-08 LT. Due to the retrograde orbit of RAE-1, for October and December, the premidnight period (20-24 LT) adds data only in the latitude range from about -50° to -60°, while the post-midnight period covers the northern hemisphere. The orbital inclination of the satellite precludes observation of geographic areas poleward of about 60° north and south geographic latitudes.

To gain full longitudinal coverage around the Earth, it was necessary to utilize noise data on consecutive orbits for a period of several days. This procedure tends to smear the

geographic distribution to some extent, because an active tropospheric weather region (such as a cold front) may generate thunderstorm activity for two or three days with some displacement in location. Even on consecutive orbits, the wide area of downward Vee coverage at Earth's surface overlays common areas and the same stormy region could conceivably be seen again if it persisted for four hours.

Another obvious limitation to the present results is that, being based upon a small sampling of data over a few days, they do not necessarily represent average conditions for either October or December.

In spite of the above limitations, the results exhibit rather striking characteristics.

Gross features apparent in both October (Fig.22) and December (Fig.23) lend credence to the assumption that the observed noise is emanating from sources at or near Earth's surface.

For example, the highest noise regions are found over the major land masses of the world (Far East, South America, Southern Africa), while the lowest noise levels are observed in mid-ocean. As a matter of fact,the noise level in the south Pacific is lower than it is in the south Atlantic ocean, at least partly because of the longer distance from continental land masses to the mid-Pacific compared to mid-Atlantic. (No contour levels below 25dB> 288°K were obtained since this is approximately the cosmic noise level on 9.18 MHz).

Comparing October (Spring in southern hemisphere) to December (Summer), a generally lower noise level is found over both land and sea in the Springtime, in agreement with the known seasonal variation in world-wide thunderstorm activity. For this comparison, it should be noted that the hatch marks in the October map cover areas having 55 dB or greater noise level, while those in December cover 60 dB or greater. The 55 dB area over the Far East is much greater in extent in Summer (Fig.23) than in Spring (Fig.22).

Other features of importance in these two maps include the appearance of localized high-noise regions over some ocean areas, notably in the Indian Ocean centered on 20° S at longitudes of 70° E and 105° E (October only). In both months (Fig 22and 23) there are distinct highs at about 5° S, 200° E and 15° S, 350° E in the Pacific and Atlantic Oceans, respectively. The mid-Pacific high (5° S, 200° E) is evident in the C.C.I.R. maps for Spring and Summer (Figs.11 and 12) but the one in the Atlantic (15° S, 350° E) is not.

Other details of the terrestrial noise distributions obtained from the RAE passes can be discerned in the October and December maps.

5.3 Discussion

The noise distribution maps presented in Figs.22 and 23 must be regarded as preliminary since they represent only a limited time

period and only the sourthern hemisphere. As mentioned, above, there is gross agreement between these distributions and those derived from ground based observations (CCIR, 1964), especially regarding the high-noise regions over continental land masses compared to the relatively low levels over oceans. There are, however, differences in detail which should be discussed.

Of prominent notice is the pronounced high-noise region over the Atlantic Ocean centered at about 15° S, 350° E. It covers the British Islands of Ascension and St. Helena, but has no distinct counterpart in either the Spring or Summer CCIR noise maps (Figs. 11 and 12). Since neither man-made radio noise nor transmitted signals have yet been isolated in the RAE data, the terrestrial noise patterns deduced here represent the composite sum of these components plus atmospherically generated radio noise. Thus, the high noise level over Ascension Island and St. Helena Islands may be due to a relatively strong contribution from man-made sources (or 9MHz signals) compared to the atmospheric noise component. Thunderstorm occurrence frequency maps (Israel and Dolezalik, 1961) show a slightly higher thunderstorm occurrence-

incidence in October than in December in this part of the world, but both occurrence rates are considerably lower (7 and 5 per 3-months) than the rates over Africa (maximum 60 in both October and December). The 55 to 65 dB level observed over the two islands is scarcely less than that in the high noise regions over Africa and Madagascar. To attribute the observed high noise level over Ascension and St. Helena to atmospheric sources, one would have to presume that thunderstorms just happened to be in progress there in both October and December as RAE passed over. For this particular high noise region, it presently appears that man-made sources are the likely cause, but before a final conclusion can be drawn, additional noise distributions at frequencies other than 9.2 MHz must be constructed and the presence of man-made sources or transmitters on these islands should be verified. It could be that the lack of a maximum region in either the CCIR noise data and the Israel-Dolezalek thunderstorm distribution is due to a lack of observations in that particular part of the world.

Following the same argument, it may be speculated that the contributions from man-made sources on continental land masses may be obscured in the RAE data by naturally occurring atmospheric radio noise emanating from thunderstorm regions. At present,

however, it is best to view the noise patterns contained in Figs. 22 and 23 as being the composite level at RAE heights produced by the joint contribution of atmospheric noise, man-made noise and radio frequency interference, although one source or another may dominate at particular times and places. Further analysis of the RAE data is required to identify the dominant source.

In regard to the accuracy in location of the maximum noise areas depicted in Figs. 22 and 23 , it will be recalled (Section 2) that even on 9.2 MHz the downward Vee antenna views a geosurface area of about 3×10^6 km^2 neglecting ionospheric cutoff effects. A single data point on the base map thus has an average maximum uncertainty in position of about $\pm 10°$ latitude and longitude. However, in utilizing a collection of data points to produce iso-noise level contours defining a spatial distribution, as was done here, the uncertainty in position should be reduced by a factor of 2 or 3. This reduction is introduced by the fact that the shape and location of a given contour are dictated by not only the individual data points nearest to it, but also by the adjacent and next 3 or 4 contour line shapes which have themselves been dictated by individual data points. If we count the first estimate of a contour shape and position as one measurement, then the subsequent refinement by the neighboring 4 contours represents four additional measurements. Since the uncertainty of measurement is decreased by $\sqrt{N}$ where N is the number of measurements

it follows that the refined position of the initial contour will have an uncertainty one-half as great as that for the first estimate. The precise amount of uncertainty reduction also depends upon the number of data points utilized for drawing each first-estimate contour line as well as the weight assigned to the neighboring contours (the more distant contours have the least weight). However, on the basis of this rather heuristic argument, we conclude that the contour lines and hence maximum noise regions depicted in Figs. 22 and 23 are correctly located to within about $\pm 5°$ in latitude and longitude except near 0° and -60° latitude where there are few data points.

In this report the absolute values of the dB contour levels are of secondary significance. The main point has been the exhibition of spatial noise patterns. However, it is of interest to compare the RAE measurements with C.C.I.R (1964) predictions, to show similarities in HF noise near Earth's surface and at 6000 km altitude. For example, the 65 dB contour in South America for December (Fig. 23) corresponds to the CCIR prediction for 00 - 04 LT in Summer in the same geographic area on this frequency. The prediction is 50 ± 7 dB, which agrees tolerably well with the measurement, especially considering that no corrections for possible ionospheric effects have been made to the RAE measurements. In the middle of the South Pacific Ocean (say at 40°S, 210°E) the measured

Summer noise level (Fig.23) is 30 dB above 288°K (or F_a=30dB), compared to the CCIR prediction of 38 $\pm$ 7dB. The relatively good agreement between measurement and prediction for both a high noise and low noise area suggest that the results presented in Fig. 23 are due principally to atmospheric radio noise.

To summarize this discussion, it appears that all the evidence investigated supports the hypothesis that the noise observed during night time on the downward Vee antenna has its origin in terrestrial sources below the ionosphere. The spatial patterns exhibiting generally high noise levels over continents and low levels over oceans, the generally lower noise level observed in October (Spring) compared to December (Summer), and the lower level in the South Pacific Ocean compared to the South Atlantic all fit the terrestrial noise hypothesis. This being the case, further analysis of the RAE downward Vee data will be exceedingly fruitful for obtaining spatial and temporal distributions of terrestrial radio noise.

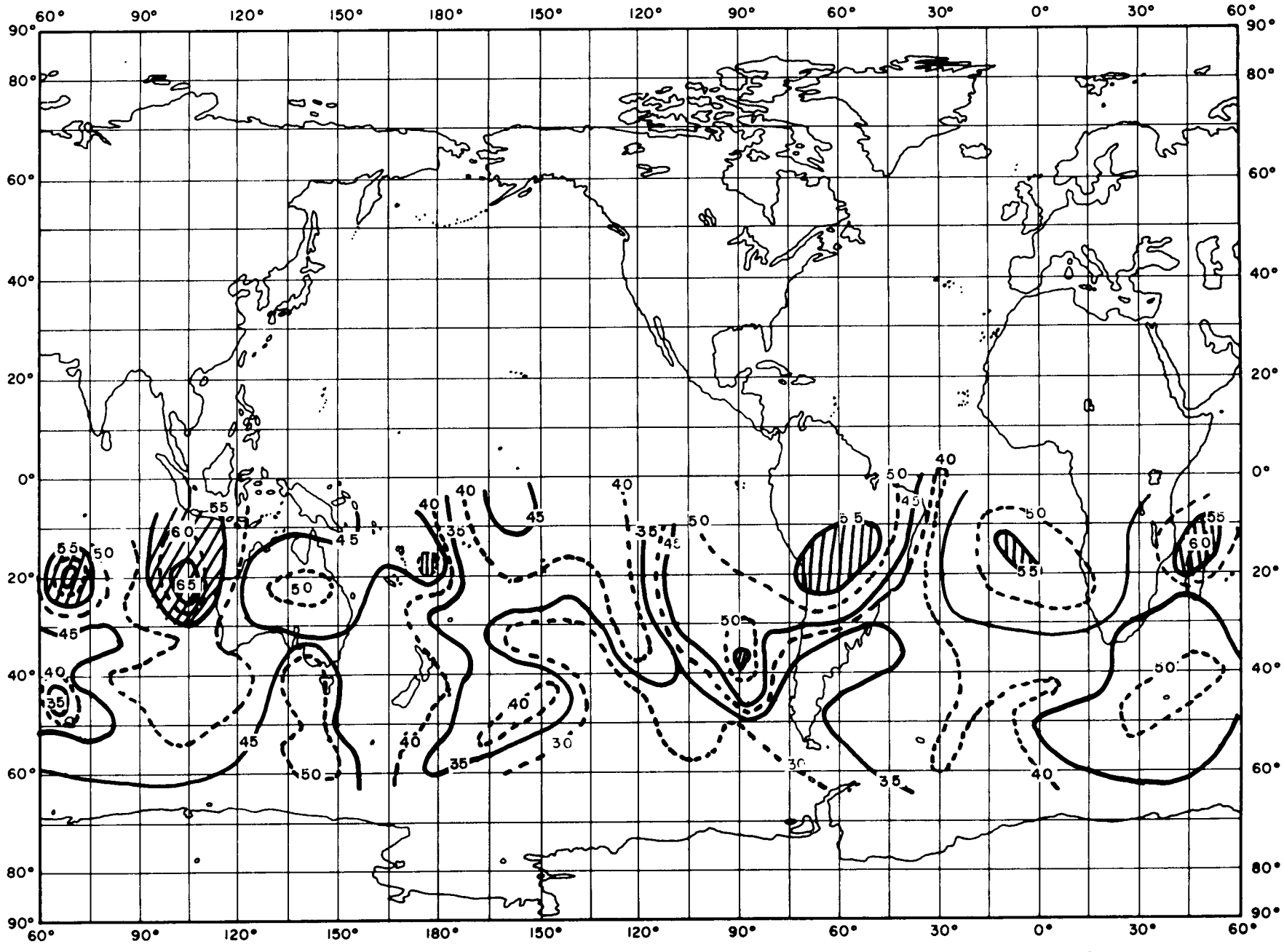

FIGURE 22 - TERRESTRIAL RADIO NOISE DISTRIBUTION DERIVED FROM RV DOWNWARD VEE DATA ON 9.18 MHz FOR OCT. 15-22, 1968, 0000-0400 LT (APPROX. 160 DATA POINTS). CONTOUR LEVELS ARE dB ABOVE 288°K.

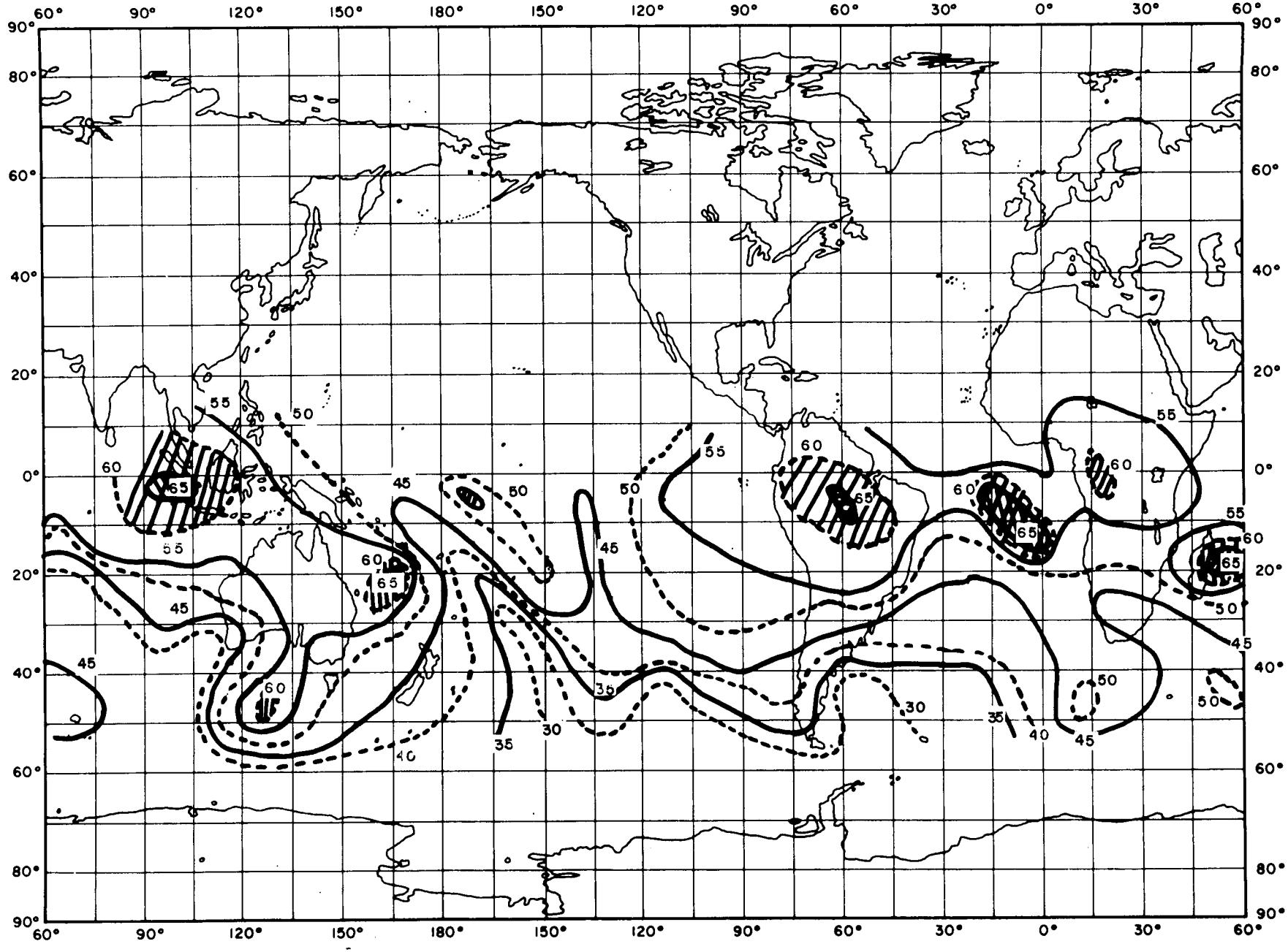

FIGURE 23 - TERRESTRIAL RADIO NOISE DISTRIBUTION DERIVED FROM RV DOWNWARD VEE DATA ON 9.18 MHz FOR DEC. 2-6, 1968, 0000-0400 LT (APPROX. 90 DATA POINTS). CONTOUR LEVELS ARE dB ABOVE 288°K.

6.0 NOISE BURSTS OF UNDETERMINED ORIGIN

Upon examining the data on the RAE I dipole burst radiometer one observes signal enhancements or energy bursts superimposed on the ambient noise background. The bursts occur on any of the frequencies within the frequency spectrum, with the bursts occurring either individually or in groups. Bursts are ordinarily 15 seconds in duration during which the satellite moves approximately 100 km along its orbit while the sub-satellite point moves 50 km. The time interval between bursts within a group ranges from 1 to 60 seconds, but occasionally only isolated cases are observed in the HF band of frequencies (such as in Fig. 13).

We have not yet identified the origin of this peculiar phenomenon, but since it occurs most often on the night side there is a possibility that it may originate near Earth's surface. Because the origin is still undertermined the phenomenon and its observed characteristics are discussed only briefly.

6.1 Possible Generation Mechanisms

Barring an equipmental generation source, several natural mechanisms suggest themselves as possibilities. These are:

a) in situ generation of plasma spikes

b) magnetospheric generation of propagating electromagnetic pulses of short duration

c) intense lightning flashes from discrete thunderstorms

d) transmitted signals of terrestrial origin

d) extraterrestrial sources

A lengthy discussion of the various possibilities is unwarrented here, but the highlights may be summarized.

If the source were in situ generation by interaction between energetic charged particles and the ambient plasma, bursts would be generated on frequencies satisfying the condition

$$1 > X > 1 - Y^2$$

where

$$X = f_p^2 / f^2$$

$$Y^2 = f_H^2 / f^2$$

f_p = plasma frequency at RAE height

f_H = electron gyrofrequency

thus the bursts would occur on frequencies bounded by

$$f_p < f < (f_p^2 + f_H^2)^{1/2}$$

Since the electron density at 6000 km is of the order 10^3 cm^{-3}, $f_p \simeq 0.3$ MHz and the upper hybrid frequency is roughly 0.8 MHz. It appears that the bursts on 3 MHz and above stems from another cause.

Individual lightning flashes generate rf signals of durations less than about 300 msec (Horner, 1965) and are insufficient to explain the 15-sec bursts.

If terrestrial transmitters were the cause, the size of the ionospheric iris allowing penetration of the signal would have to be very small ($\sim$ 100 km), indicating that foF2 would

have to be .995 of the observing frequency (Fig. 4). However, the bursts are seen nearly as often over oceans as over land. There is a possibility that HF signals would be trapped in magnetospheric ducts in a manner similar to that discussed by Muldrew (1967), after penetration through an irregular F region (Herman, 1966). The RAE would observe the trapped signal only while traversing the magnetospheric duct. This possibility has not been ruled out altogether, but is still completely unverified.

6.2 Observed Characteristics

A typical example of a group of bursts is displayed in Fig. 24. The bursts are seen to be of 15 second durations with a spacing of 30 seconds. In this particular example the bursts occur only on 4.94 and 5.41 MHz.

Analysis of the Ryle-Vonberg Radiometer data for comparable time periods reveals the occurrence of what appears to be the result of the same phenomenon. The plots of noise temperature versus time at a given frequency consist of a series of points, each point representing data averaged over a 32 sec period. Typically, one observes a relatively smooth curve with discrete high amplitude "spikes" occurring at apparently random times. The spikes consist of a cluster of either one, two or three points at a much higher noise temperature than the temperature of the continuum curve. An example of this feature can be seen in Fig. 17 on 4.7 MHz at 1448 UT.

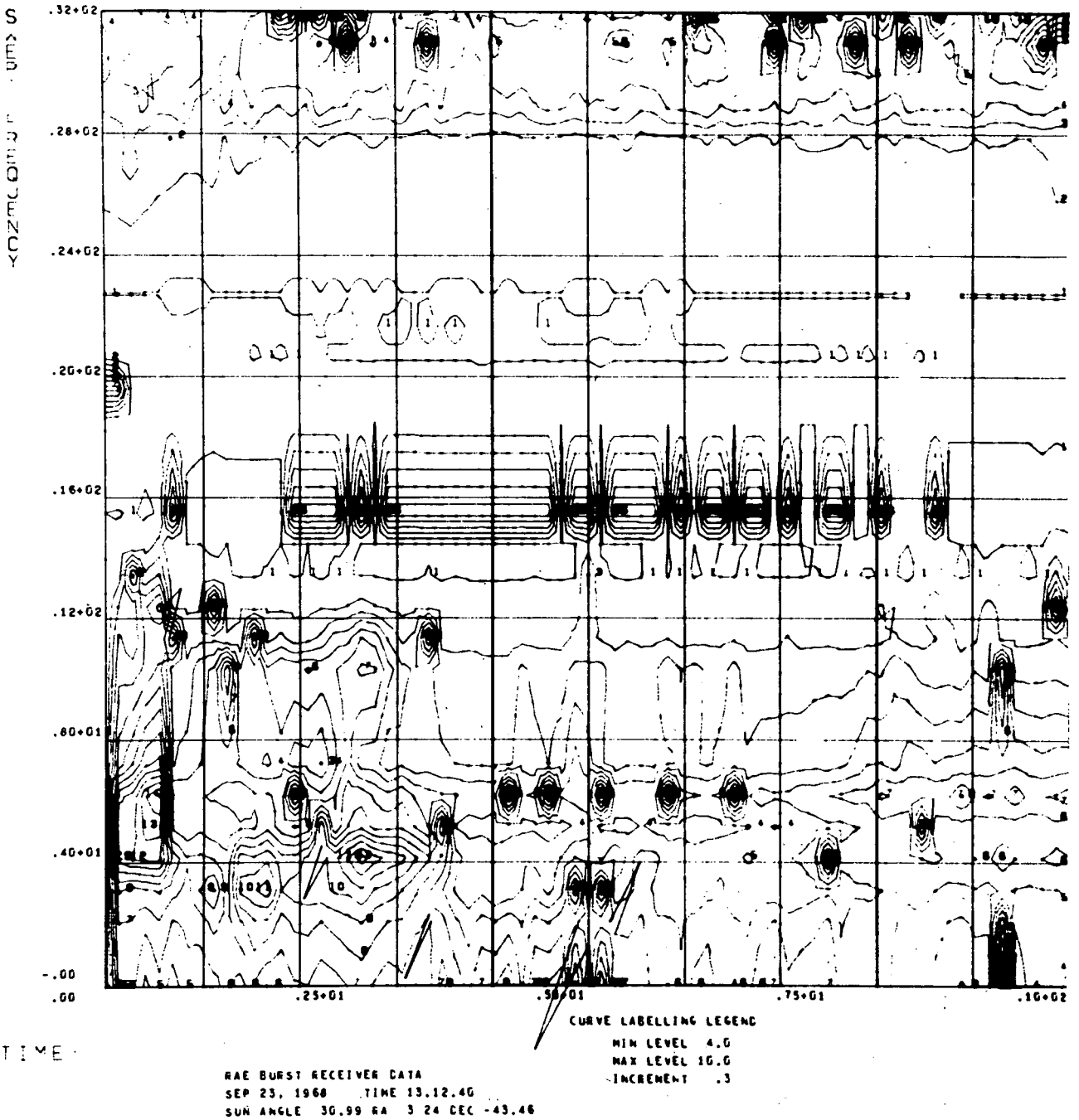

FIGURE 24 - BR SWEEP FREQUENCY DATA WITH SHORT DURATION BURSTS AT HIGH FREQUENCY.

If the spikes on the Ryle-Vonberg display do in fact correspond to the 15 second bursts mentioned above, one expects that individual bursts separated by more than 30 seconds would have a high probability of being averaged out over the 32 sec averaging period. Consequently, one would expect to see less bursts on the Ryle-Vonberg display. An examination of a small sampling of data reveals that this appears to be the case.

If one plots the geographic distribution of bursts for both the RV and BR data, one would expect comparably shaped distribution plots although the total number of bursts may be different. This is, of course, assuming that both types of burst are a result of the same mechanism. Figure 25 is a plot of number of bursts as a function of latitude for a period in December, 1968 for both the RV and BR data. As can be seen from the figure, the bar graphs are quite similar. On the basis of the distribution plots and the evidence presented above, it is felt that the bursts on both displays are equivalent.

Distribution plots for 3 additional time periods are also presented in Figure 25. In October, November and December, the number of bursts are evenly distributed over both the northern and southern hemisphere. However, in August the

density of bursts is greater in the southern hemisphere which corresponds to the night side of the satellite path. If the number of bursts are plotted as a function of longitude for the same time periods the result is a uniform distribution of bursts. This implies that the bursts are independent of longitude, at least for the periods investigated.

Briefly summarizing, high energy bursts are observable on both the BR and RV data. The bursts occur in apparently random fashion which would indicate that they are not a result of equipment malfunction or calibration procedures. The BR bursts correspond to RV bursts and, therefore, apparently originate from the same source. At this point the results are inconclusive and require a more detailed study.

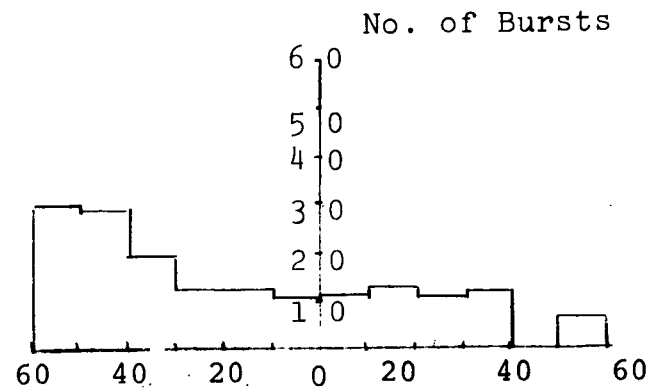

AUGUST 10, 1068 BR DATA

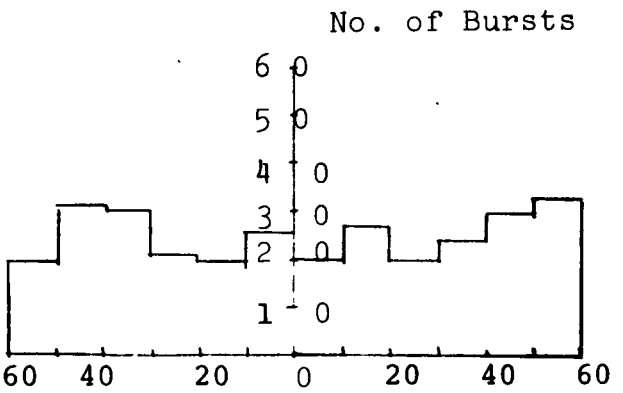

OCTOBER 17, 1968 BR DATA

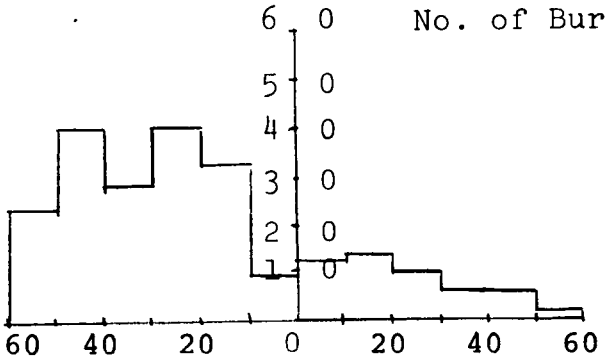

AUGUST 29, 1968 BR DATA

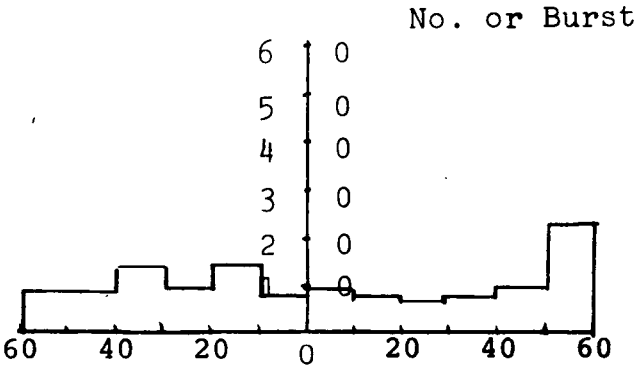

DECEMBER 3, 1968 BR DATA

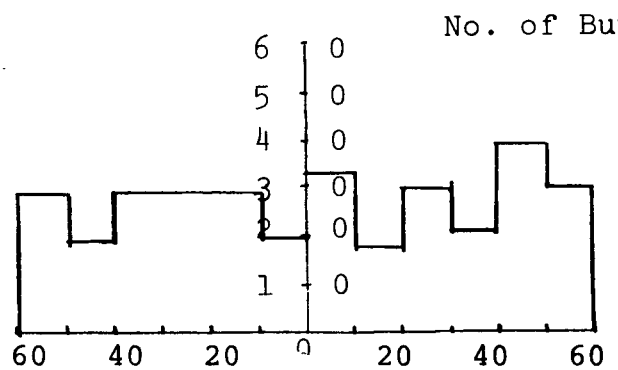

NOVEMBER 2-3, 1968 BR DATA

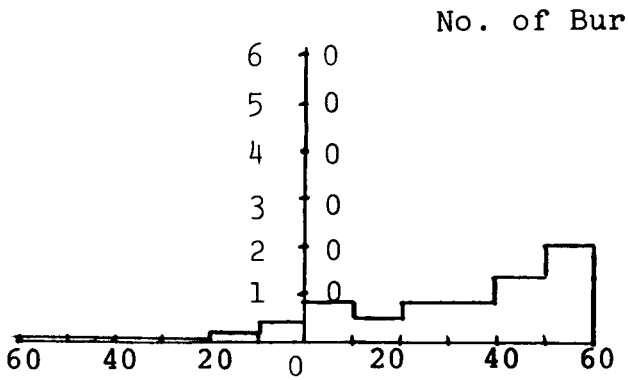

DECEMBER 2-3, 1968 RV DATA

FIGURE 25 - LATITUDINAL DISTRIBUTION
OF NUMBER OF BURST OCCURRENCES OBSERVED
BY BR AND RV RECEIVERS

7.0 CONCLUSIONS

Investigation of certain features of radio noise observed by RAE I on its dipole and downward Vee antennas has revealed that a significant amount of terrestrially generated noise will at times penetrate through the ionosphere to 6000 km altitude. This noise can be at least 15 dB above the cosmic noise background but the upper limit cannot be ascertained due to receiver saturation.

As the satellite approaches a region of low peak ionospheric electron density (critical frequency) terrestrial noise in excess of cosmic noise on successively lower frequencies is received by RAE, producing the typical "ground breakthrough" pattern observed in the dipole antenna sweep frequency data. Terrestrial noise is usually observed by RAE over the night side of the Earth or at high declination angles where foF2 is low.

Fixed frequency data from the Ryle-Vonberg receivers on the downward Vee antenna reveal that the terrestrial noise level is lowest when RAE is over oceans and highest when it is over equatorial land masses where thunderstorm activity is most prevalent. Geographic distributions for periods in October and December, 1968, of the terrestrial noise as observed by RAE are similar to distributions derived from ground-based noise data taken over a period of years.

It appears that a qualitative model taking into account the spatial and temporal variations in both terrestrial noise source distributions and ionospheric critical frequencies, is adequate to explain the gross features of the terrestrial noise component observed in the RAE data. The magnitude of noise available to penetrate through the ionosphere from any point on the Earth's surface is the total of all contributions from thunderstorms, urban noise centers or terrestrial transmitters that originate or have arrived at that point after propagation over an appropriate distance via ionospheric reflections or groundwave propagation. Based on this model, the noise level over the oceans in locations well removed from noise sources is lower than it is over continental land masses. The RAE observations are in agreement with this model.

8.0 REFERENCES

Aiya, S.V.C., Noise Power radiated by tropical thunderstorms, Proc. I.R.E., 43, 966, 1955.

C.C.I.R., World-Wide Atmospheric Radio Noise Predictions, C.C.I.R. Report No. 65, International Radio Consultative Committee, Geneva, 1957.

C.C.I.R., World Distribution and Characteristics of Atmospheric Radio Noise, C.C.I.R Report No. 322, International Radio Consultative Committee, Geneva, 1964.

Crichlow, W.Q., D. F. Smith, R. N. Morton and W. R. Corliss, "Worldwide Radio Noise Levels Expected in the Frequency Band 10 Kilocycles to 100 Megacycles," NBS Circular 557, August 25, 1955.

Davies, K., "Ionospheric Radio Propagation," National Bureau of Standards Monograph 80, U. S. Govt. Printing Office, Washington, 1965.

ESSA, Ionospheric Predictions (monthly), Environmental Science Services Administration, 1968.

Herman, John R., A Sensitive Technique for Detecting Late Time Absorption Following High Altitude Nuclear Explosions, Radio Science, 3, 964-973, 1968.

Herman, John R., A Survey of Man Made Radio Noise, Review paper presented at URSI General Assembly, Ottawa, 1969.

Horner, F., A Review of Information on Atmospherics From Near Lightning Discharges, in Radio Noise of Terrestrial Origin. (F. Horner, Ed.) Elsevier Publishing Co., Amsterdam, 85, 1962.

Horner, F.,Radio Noise In Space Originating In Natural Terrestrial Sources, Planet Space Sci., 13, 1137-1150, 1965.

Huguenin, G.R., and M. D. Pappagiannis, Spaceborne Observations Of Radio Noise From 0.7 to 7.0 MHz and Their Dependence In The Terrestrial Environment, Ann. Astrophys., 28, 239, 1965.

Israël, H. and H. Dolezalek, "Atmosphärische Elektrizität, Part 2, Geest und Portig K.-G., Leipzig, 1961.

Kaiser, M.L., Radio Astronomy Explorer-1 Data Displays, Goddard Space Flight Center Rpt. X-693-70-326, August, 1970.

Krumm, H.=Chr., "Der Weltzeitliche Tagesgang der Gewitterhäufigkeit," Zeitschrift fur Geophysik 28 (No. 2) 85-104, 1962.

Lipson, S. G., and H. Lipson, Optical Physics, Cambridge Univ. Press, 1969.

Muldrew, D. B., MF Conjugate Echoes Observed on Alouette 2 Topside Sounder data, Canad. J.Phys., 45, 3935-3944, 1967.

Rawer, K., Noise Produced by Terrestrial Sources in the Near-Earth Space, in Propagation Factors in Space Communications, (W.T. Blackband, ed.), McKay and Co., London, 383-408, 1967.

Sparrow, J. G. and E. P. Ney, Lightning Observations by Satellite, Nature,232, 540-541, 1971

Stone, R.G., Research Results from the Radio Astronomy Explorer, AIAA 6th Annual Meeting, Anaheim, California, Paper No. 69-1049, October 20-24, 1969.

Weber, R.R., J. K. Alexander, and R. G. Stone, The Radio Astronomy Explorer Satellite; A Law Frequency Observatory, Goddard Space Flight Center, Preprint X-693-71-64, June, 1971.

Whipple, E.J.W., "On the Association of the Diurnal Variation of Electric Potential Gradient in Fine Weather with the Distribution of Thunderstorms over the Globe," Quart. J., R. Met. Soc. 55, 1-13, 1929.